

國立交通大學

機械工程學系

碩士論文

微步進機構定位之研究

The Research of Positioning for

Micro-stepping Mechanism



研究生：陳立明

指導教授：成維華 教授

中華民國九十四年六月

微步進機構定位之研究

The Research of Positioning for
Micro-stepping Mechanism

研究生：陳立明

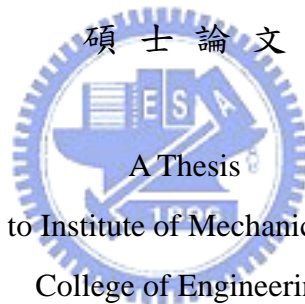
Student : Li-Ming Chen

指導教授：成維華

Advisor : Wei-Hua Chieng

國立交通大學

機械工程學系



Submitted to Institute of Mechanical Engineering
College of Engineering

National Chiao Tung University

in partial Fulfillment of the Requirements

for the Degree of

Master

in

Mechanical Engineering

June 2005

Hsinchu, Taiwan, Republic of China

中華民國九十四年六月

微步進機構定位之研究

研究生：陳立明

指導教授：成維華 教授

國立交通大學機械工程學系

摘要

微步進是一種設計用來增加工作行程精密定位的機構。我們選擇壓電材料其對應驅動電壓而快速伸縮的特性，以建構出一種利用黏滯與滑動的摩擦機制產生運動之衝量驅動機構。當施加不對稱的驅動電壓波形，會造成壓電材料帶動整體機構作週期性的步進運動。雖然如此，目前仍存在著許多問題。因為量測極微小的位移量，這類機構對環境上的變化相當敏感，尤其是滑塊與導軌間存在著不確定性的摩擦分布影響甚大。具有預滑動之摩擦模型與質量-阻尼-彈簧之衝量機構模型在此被提出討論，用以分析此機構之動力學。首先改良先前微步進機構之缺點，設計一個新的機構，之後結合 DSP 控制器與雷射干涉儀測量系統作實驗上步進之驗證，以探討驅動的控制波型對精密定位之影響。此外，研究中發現另一種驅動微步進機構的方法，可以實際應用在長程的定位方面。

The Research of Positioning for Micro-stepping Mechanism

Student: Li-Ming Chen

Advisor: Dr. Wei-Hua Chieng

Institute of Mechanical Engineering
National Chiao Tung University

Abstract

Micro-stepping mechanism is designed to expand the working stroke for precise positioning. A piezoelectric material is chosen to construct the impact drive mechanism, a stick-slip type of mechanism utilizing contact frictional force by rapid displacement response. Applying asymmetric driving waveforms to the piezoelectric element makes the mechanism move step by step periodically. However, many complicated problems exist. Due to such an extremely small displacement, the mechanism is very sensitive to changes in the surroundings, especially the indeterminate distribution of friction between the slider and the guide surface. A linearized mass-damper-spring model with pre-sliding friction is constructed to investigate the dynamics of the mechanism. By improving the previous structure of the mechanism, we will combine the DSP controller and the interferometer measuring system to verify the stepping of the mechanism experimentally. The influence of different control waveforms is discussed. In addition, a new discovered driving method in the research may be used well for long traveling in practice.

Acknowledgements

First, I wish to express my gratitude to my advisor, Prof. Wei-Hua Chieng, who gave me many valuable comments and helpful suggestions during my graduate career. I am also indebted to all the seniors of Intelligent Mechtronical Lab for their assistance and guidance in the study, especially to Kuo-Liang Chang and Yong-Chieng Tong. Without their help, the research will not be completed. Finally, I would like to thank my family and friends who support and inspire me in my school life. The time with them is always full of happiness. Thanks very much.



Contents

摘要	i
Abstract	ii
Acknowledgements.....	iii
Contents.....	iv
List of Figures	v
List of Tables	vii
Chapter 1 Introduction	1
1.1 Piezoelectricity	1
1.2 History	2
1.3 Motive.....	4
1.4 Research Orientation	5
Chapter 2 Micro-Stepping Mechanism Using Piezoelectric Actuators.....	7
2.1 Non-linearity of Piezoelectric Actuators.....	7
2.2 Micro-Stepping Mechanism Overview	9
2.3 Review of Impact Drive mechanism	10
2.4 Operating Principle of Impact Drive Mechanism.....	12
2.5 Models of Impact Drive Mechanism	13
2.5.1 Rigid Body Model	13
2.5.2 Mass-Damper-Spring Model	14
Chapter 3 Experiment	21
3.1 Improvement of IDM	21
3.2 Experimental Setup	22
3.3 DSP Program Flowchart	23
3.4 Experimental Results	25
3.5 Observation of Forward and Backward Movement	27
3.6 Discovery of IDM.....	28
Chapter 4 Conclusion.....	29
Reference	31

List of Figures

Figure 1.1 Piezoelectric effect and its reversibility.....	34
Figure 1.2 Perovskite structure	34
Figure 2.1 Hysteresis curves of an open loop piezoelectric actuator.....	35
Figure 2.2 Creep of an open loop piezoelectric actuator	35
Figure 2.3 Classification of piezoelectric positioning device	36
Figure 2.4 Operating principle of IDM	37
Figure 2.5 The rigid body of model of IDM	38
Figure 2.6 The mass-damper-spring model of IDM	38
Figure 2.7 The typical input pattern for IDM	38
Figure 3.1 Previous IDM structure.....	39
Figure 3.2 Advanced IDM structure.....	39
Figure 3.3 P-840.10 preloaded LVPZT translator.....	39
Figure 3.4 Structure for measurement.....	40
Figure 3.5 System configuration	41
Figure 3.6 Experiment setup	42
Figure 3.7 Impact drive mechanism.....	42
Figure 3.8 DSP module	43
Figure 3.9 2407A device architecture	43
Figure 3.10 Functional block diagram of the 2407A DSP controller	44
Figure 3.11 Program flow	45
Figure 3.12 100V, 100Hz, 95% duty input, displacement of the counter-mass	46

Figure 3.13 100V, 300Hz, 95% duty input, displacement of the counter-mass	46
Figure 3.14 100V, 500Hz, 95% duty input, displacement of the counter-mass	47
Figure 3.15 100V, 900Hz, 95% duty input, displacement of the counter-mass	47
Figure 3.16 100V, 100Hz, 95% duty input, displacement of the slider	48
Figure 3.17 100V, 300Hz, 95% duty input, displacement of the slider	48
Figure 3.18 100V, 500Hz, 95% duty input, displacement of the slider	49
Figure 3.19 100V, 900Hz, 95% duty input, displacement of the slider	49
Figure 3.20 100V, 100Hz, 95% duty input, standard step of the slider	50
Figure 3.21 100V, 100Hz, 95% duty input, standard step of the counter-mass	50
Figure 3.22 (a) 60V; (b) 80V; (c) 100V, 100Hz, 95% duty input, displacement of the slider	51
Figure 3.23 (a) 60V; (b) 80V; (c) 100V, 100Hz, 5% duty input, displacement of the slider	52
Figure 3.24 Forward displacement of the slider, 100Hz	53
Figure 3.25 Backward displacement of the slider, 100Hz	53
Figure 3.26 50V, 1400Hz, sine waveform input, displacement of the slider ..	54
Figure 3.27 Velocity of the slider with various sine waveforms.....	54

List of Tables

Table 3.1 Technical data of P-840.10 preloaded LVPZT translator..... 55



Chapter 1 Introduction

1.1 Piezoelectricity

Piezoelectricity is the ability of certain crystals to produce a voltage when subjected to mechanical stress. The word is derived from the Greek “piezo”, which means to squeeze or press. Piezoelectricity is a linear effect that is related to the microscopic structure of the solid. Some ceramic materials become electrically polarized when they are strained. This linear and reversible phenomenon is referred to as the direct piezoelectric effect. Piezoelectric materials also show the opposite effect, called the converse piezoelectricity. Figure 1.1 demonstrates the connection between electrical and mechanical domains. An electrical field creates mechanical stress (distortion) in the crystal structure because the charges inside the crystal are separated. The applied voltage affects different points within the crystal differently, resulting in the distortion. The microscopic origin of the piezoelectric effect is the displacement of ionic charges within a crystal structure. In the absence of external strain, the charge distribution within the crystal is symmetric and the net electric dipole moment is zero. However, when an external stress is applied, the charges are displaced and the charge distribution is no longer symmetric. A net polarization develops and results in an internal electric field. A material can only be piezoelectric if the unit cell has no center of inversion. The effect is of the order of nanometers, but nevertheless finds useful applications such as the production and detection of sound, generation of high voltages, electronic frequency generation, and

ultrafine focusing of optical assemblies.

1.2 History

In 1880, the brothers Pierre Curie and Jacques Curie predicted and demonstrated piezoelectricity using tinfoil, glue, wire, magnets, and a jeweler's saw. They showed that crystals of tourmaline, quartz, topaz, cane sugar, and Rochelle salt (sodium potassium tartrate tetrahydrate) generate electrical polarization from mechanical stress. Quartz and Rochelle salt exhibited the most piezoelectricity. Twenty natural crystal classes exhibit direct piezoelectricity. In 1881, the term "piezoelectricity" was first suggested by W. Hankel, and the converse piezoelectricity was mathematically deduced by Lipmann from fundamental thermodynamic principles. The Curies immediately confirmed the existence of the "converse effect," and went on to obtain quantitative proof of the complete reversibility of electro-elasto-mechanical deformations in piezoelectric crystals.

In the next three decades, collaborations within the European scientific community established the field of piezoelectricity; and by 1910, Voigt's "Lerbuch der Kristallphysic" was published and became a standard reference work detailing the complex electromechanical relationships in piezoelectric crystals. However, the complexity of the science of piezoelectricity made it difficult for it to mature to an application until a few years later. The first practical application for piezoelectric devices was sonar, first developed during World War I. In France in 1917, Langevin et al. developed an ultrasonic submarine detector. The detector consisted of a transducer, made of

thin quartz crystals carefully glued between two steel plates, and a hydrophone to detect the returned echo. By emitting a high-frequency chirp from the transducer, and measuring the amount of time it takes to hear an echo from the sound waves bouncing off an object, one can calculate the distance to that object. Their success opened up opportunities for intense development interest in piezoelectric devices. Over the next few decades, new piezoelectric materials and new applications for those materials were explored and developed. In 1935, Busch and Scherrer discovered piezoelectricity in potassium dihydrogen phosphate (KDP). The KDP family was the first major family of piezoelectrics and ferroelectrics to be discovered.

During World War II, research in piezoelectric materials expanded to the U.S., the Soviet Union and Japan. Up until then, limited performance by these materials inhibited commercialization but that changed when a major breakthrough came with the discovery of barium titanate and lead zirconate titanate (PZT) in the 1940s and 1950s respectively. These families of materials exhibited very high dielectric and piezoelectric properties. Furthermore, they offered the possibility of tailoring their behavior to specific responses and applications by the use of dopants. Starting around 1965, several Japanese companies focused on developing new processes and applications, and opening new commercial markets for piezoelectric devices. The success of the Japanese effort attracted other nations.

Today, PZT is one of the most widely used piezoelectric materials. It is noted that most commercially available ceramics (such as barium titanate and PZT) are based on the perovskite structure shown in Figure 1.2. The perovskite structure (ABO_3) is the simplest arrangement where the corner-sharing oxygen octahedra are linked together in a regular cubic array

with smaller cations (Ti, Zr, Sn, Nb etc.) occupying the central octahedral B-site, and larger cations (Pb, Ba, Sr, Ca, Na etc.) filling the interstices between octahedra in the larger A-site. Compounds such as BaTiO₃, PbTiO₃, PbZrO₃, NaNbO₃ and KNbO₃ have been studied at length and their high temperature ferroelectric and antiferroelectric phases have been extensively exploited. This structure also allows for multiple substitutions on the A-site and B-site resulting in a number of useful though more complex compounds such as (Ba,Sr)TiO₃, (Pb,Sr)(Zr,Ti)O₃, Pb(Fe,Ta)O₃, (KBi)TiO₃ etc.

1.3 Motive

To date, the needs and uses of piezoelectric devices extend from medical applications to the communications field to military applications and the automotive field. Piezoelectric materials are well known for great rigidity, low power consumption, rapid response, and ultra-high resolution. As very high voltages correspond to only tiny changes in the width of the crystal, this width can be changed with better-than-micrometer precision, making piezo crystals the most important tool for positioning objects with extreme accuracy. Due to the piezoelectric effect and these excellent features, piezoelectric ceramics are commercially available devices for measuring displacements in the range of 10pm to 100um. These applications include optical fiber alignment, mask alignment, scanning electron microscope, focusing and tracking of a hard disk drive, etc. Thus, we look forward to construct a new design of the micro-stepping mechanism with piezoelectric actuators to achieve the accuracy of positioning.

1.4 Research Orientation

First, the non-linearity of piezoelectric actuators is introduced. The non-linear effects between the input voltage waveform and the output deformation cause undesirable inaccuracy especially hysteresis. It brings about a rate-independent lag phenomenon and residual displacement near zero input. These phenomena reduce the accuracy of the actuators and result in poor performance in the piezoelectric actuator which is operated in open-loop mode.

The main purpose is to design a mechanism of the piezoelectric actuator in precise positioning with long traveling displacement. We choose the piezoelectric impact drive mechanism (IDM) which belongs to stick-slip actuators of the pulse type for experiment. To expand the working range of stroke with high resolution, a voltage amplifier is necessarily needed. IDM is one type of micro-stepping device that can achieve nanometer resolution. The operating principle of the impact drive mechanism is explained. Applying an asymmetric voltage waveform to piezoelectric elements which is connected to the slider and the counter-mass of IDM causes a series of motions on the guide way. The piezoelectric elements used to excite each stepping motion of IDM are considered to be a linear and rigid device that can provide a fast displacement response. A mass-damper-spring model is constructed to investigate the dynamics of the mechanism.

An experimental environment, based on the laser interferometer, is set up for managing the displacement of the piezoelectric actuator. After data converting reference and measurement signals from laser head and

measurement receiver, the information is processed by DSP which provides fast digital input read operation. The DSP module can also produce driving waveforms needed in the experiment at the same time. With experimental results, we can observe the relation between the input voltage waveform and the output deformation then make a conclusion.



Chapter 2 Micro-Stepping Mechanism Using Piezoelectric Actuators

2.1 Non-linearity of Piezoelectric Actuators

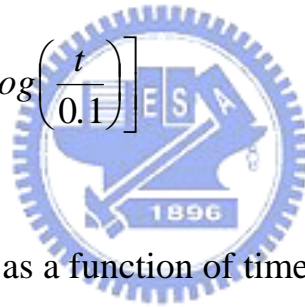
In addition to the simple mechanical structure, other beneficial general properties of piezoelectric actuators are: a short response time, an ability to create high forces, a high efficiency and a high mechanical durability. On the disadvantage side, piezoelectric actuators have small strains: only 0.1- 0.2%. Other disadvantages are a high supply voltage needed – typically between 60 and 1000V, a large hysteresis and creep (drift). Figure 2.1 presents a typical hysteresis and Figure 2.2 appears a typical drift of a piezoelectric actuator. Generally, non-linearity of piezoelectric actuators may cause undesirable inaccuracy.

The absolute displacement generated by an open-loop PZT depends on the applied voltage and the piezo gain, which is related to the remanent polarization. Since the remanent polarization, and therefore the piezo gain, is affected by the electric field applied to the piezo, the deflection depends on whether the PZT was previously operated at higher or lower field strength (and some other factors). In other words, the hysteresis behavior means that there is no unique output deformation for a certain input voltage because the output also depends on the input history. Hysteresis is typically on the order of 10% to 15% of the commanded motion. For example, if the drive voltage of a 50 μm piezoelectric actuator is changed by 10%, (equivalent to about 5 μm displacement) the position repeatability is still on the order of 1% full

travel or better than 1 μm . Classical motor-driven leadscrew positioners will have difficulty beating this repeatability.

Creep only occurs in open-loop operation, and can be eliminated by servo-control. Like hysteresis, creep is related to the effect of the applied voltage on the remanent polarization of the piezo ceramics. Creep is the expression of the slow realignment of the crystal domains in a constant electric field over time. If the operating voltage of a PZT is changed, after the voltage change is complete, the remanent polarization (piezo gain) continues to change, manifesting itself in a slow creep. The rate of creep decreases logarithmically with time. The following equation describes this effect:

$$\Delta L(t) \approx \Delta L_{t=0.1} \left[1 + \gamma \cdot \log\left(\frac{t}{0.1}\right) \right] \quad (2-1)$$



Creep of PZT motion as a function of time.

where:

$\Delta L(t)$ = creep as a function of time [m]

$\Delta L_{t=0.1}$ = displacement 0.1 sec after the voltage change is complete [m].

γ = creep factor, which is dependent on the properties of the actuator (on the order of 0.01 to 0.02 which is 1 to 2% per decade).

Maximum creep (after a few hours) can add up to a few percent of the commanded motion.

Aging refers to reduced piezo gain, among other things as a result of the depoling process. Aging can be an issue for sensor or charge-generation applications (direct piezo effect), but with actuator applications it is negligible

because repoling occurs every time a higher electric field is applied to the actuator material in the poling direction.

2.2 Micro-Stepping Mechanism Overview

Many types of piezoelectric precision positioning systems have been proposed for industrial and scientific applications. Figure 2.3 lists the typical classifications of these systems. Scanning devices produce motion by direct driven or mechanical amplified. Pulse devices include stick-slip and other types of clamping mechanism. The stick-slip device which is based on the rapid response of continuous driving voltage can generate stable stepping motion from mechanical excitation of the piezoelectric device. The stick-slip behavior results from the contact friction between the movable part and the guide surface. The third type of piezoelectric positioning system is the ultrasonic motor. The acoustic wave produced by resonantly excite piezoelectric materials induces the mechanical movement.

The pulse device seems to solve the problem of limited stroke of the scanning device. However, some bottlenecks remain.

(1) The load capacity of the pulse device, especially the stick-slip device, is low. The load variation dramatically changes the behavior of the mechanism.

(2) The stick-slip is sensitive to changes in the surroundings, such as the indeterminate distribution of friction on the guide surface, the tilting of the guide surface and mechanical vibration.

(3) The closed loop operation of the stick-slip device has not been well

developed. Current applications of stick-slip devices are based on open loop operation.

(4) The mechanism and controller must be carefully designed. A stick-slip device operated at high frequency will be out of control in a poorly damped system.

Although several disadvantages affect the application of stick-slip devices, their simple structure and effective precise positioning are the main object of the research.

2.3 Review of Impact Drive mechanism

The development of impact drive mechanism began with the design of a finely adjustable specimen holder for SEMs/STMs in the 1980s. T. Higuchi et al. proposed a prototype IDM and applied it in the design of a micro robot that serves as an inserted capillary in a cell-operation [1]. Simplified kinematics analysis was performed and the basic principle of operation of IDM was thus elucidated. S. Ling et al. used MCK model to study numerically a push-pull IDM [2]. They treated IDM simply as a velocity drive and considered only the effect of the amplitude and the frequency of input waveform on the mean velocity of IDM. All of the analysis and simulation was based on a specific IDM construction. The design parameters of IDM and the induced stepping behavior of IDM were thoroughly analyzed.

The stick-slip operation of IDM is dominated by the energy dissipation of the system, some of which results from the contact friction between the slider and the guide surface. K. Furutani et al. studied the effect of lubrication

on IDM [3]. They discussed the motion of IDM based on Newton mechanics. An approximate estimate of the motion of IDM under a specific exciting waveform pattern was provided. Four guide-surface conditions – dry, lubricated by EDF-K, Oil 32 and Oil 68 – were experimentally studied. Surface condition did not apparently affect the behavior of IDM. The critical effect of the dissipation of energy in the system is not discussed.

The application of IDM to multi D.O.F. positioning has also been extensively discussed. J. Mendes et al. constructed a planar positioning machine to finely position a print board on a work plane [4]. They used a group of six IDMs in a plane to push a work piece in the X and Y directions. The path planning of the work piece which uses six actuators was performed. Image feedback was used to achieve closed-loop position control. The mechanism was based on the robotic “Pushing Operation” of M. Mason et al. [5][6][7]. Y. Yamagata et al. proposed a similar approach [8]. They used a multi D.O.F. IDM on the end effector of a robot arm to perform automatic, precise assembly. K. Furutani et al. used IDM to develop a precision electrical discharge machine (EDM) [9][10]. They constructed an X-Y-Z- θ movable electrode-feeding device. The electrode was carried with the planar IDM. The path planning of the planer IDM-driven electrode was also accomplished.

Many clamping mechanisms were introduced to “increase” the friction force between the slider and the guide surface during the “sticking phase” of the operation of IDM to improve the poor controllability and repeatability of the stick-slip motion. K. Ikuta et al. proposed a kind of IDM using electromagnetic clamping [11]. The slider is electromagnetically clamped during the sticking phase and released during the slip phase. An extra D.O.F. of control of the electromagnetic coil was introduced. T. Idogaki et al. used a

preload spring to clamp the slider to the guide surface of IDM [12]. The passive preload exerts a larger normal force between the contact surface of the slider and the guide of IDM.

The piezoelectric material-based IDM was selected as the precise positioning in this research. The following sections emphasize on the operation and stepping behavior of IDM.

2.4 Operating Principle of Impact Drive Mechanism

Figure 2.4 describes the input waveform pattern corresponding to the movement of one dimensional linear positioning device. The slider is put on a surface and held by the friction force. A counter-mass is connected to the main object via one piezoelectric element. Controlling extension or contraction of the piezoelectric actuator by applying voltage waveforms to the piezoelectric actuator, the mechanism will move. Figure 2.4(a) represents a control method of deformations of the piezoelectric actuator for backward movement.

(1) A movement cycle begins with the original length of the piezoelectric actuator and the mechanism is stationary at start.

(2) A steep rising voltage is applied. The piezoelectric actuator makes a rapid extension and the slider moves backward and the counter-mass forward.

(3) While returning, the counter-mass should be accelerated by a constant acceleration which causes inertial force less than the static friction force. Otherwise, the slider makes reverse movement.

(4) By the time the piezoelectric actuator is contracted to the length of

the beginning, a sudden stop is happened. This action is just like a collision of the counter-mass and the slider. So the whole system starts moving backward against friction force until it loses its kinetic energy.

(5) IDM stops and the piezoelectric actuator recovers itself.

The cycle is completed through (1) to (5). Therefore, IDM can move a long distance by repeating this cycle. The same may be said, no doubt, of forward movement as shown in Figure 2.4(b).

2.5 Models of Impact Drive Mechanism

The piezoelectric impact drive mechanism (IDM) based on stick-slip motion excited by the rapid deformation of piezoelectric elements is one type of micro-stepping mechanism. Applying an asymmetric driving waveform to piezoelectric elements connected to the slider and the counter-mass of IDM causes a series of stick-slip motions between the slider and the guide surface. To examine the dynamic of stick-slip motion of IDM, piezoelectric elements are usually considered to be linear and rigid displacement devices that provide a fast response. The non-linearity of hysteresis and creep is initially neglected in the analysis. A rigid body model and a mass-damper-spring (MCK) model are introduced to reconstruct the physical behavior of IDM.

2.5.1 Rigid Body Model

Figure 2.5 shows the rigid body of IDM. For simplicity, the contact friction between the slider and the guide surface is initially considered to be

Coulomb friction. In the rigid diagram, x_1 and x_2 indicate the displacement of the slider and the counter-mass of IDM respectively; l represents the displacement of the piezoelectric element; M and m are the mass of the slider and the counter-mass; μ is the coefficient of Coulomb friction; g is the acceleration of gravity and F_p is the force exerted by the piezoelectric element. With the assumption and description, the rigid model of IDM is expressed as follows.

$$\begin{cases} M\ddot{x}_1 = -\mu(M + m)g \cdot \text{sign}(\dot{x}) + F_p \\ m\ddot{x}_2 = -F_p \\ x_2 = x_1 + l \end{cases} \quad (2-2)$$

The behavior of IDM approximates to the conservation of momentum proposed by K. Furutani et al [3]. Based on the assumption of Coulomb friction contact, the stick-slip condition of the slider during a single cycle can be analyzed with distinct input waveform. ΔL is the maximum displacement of the piezoelectric element. The maximum movement of the slider Δx during the rapid deformation of a single pulse can be predicted to be

$$\Delta x = \frac{m}{M + m} \Delta L \quad (2-3)$$

2.5.2 Mass-Damper-Spring Model

The mass-damper-spring model of IDM shown in Figure 2.6 is expressed as follows.

$$\begin{cases} M\ddot{x}_1 + c(\dot{x}_1 + \dot{l} - \dot{x}_2) + k(x_1 + l - x_2) = F_\mu \\ m\ddot{x}_2 + c(\dot{x}_2 - \dot{l} - \dot{x}_1) + k(x_2 - l - x_1) = 0 \end{cases} \quad (2-4)$$

The piezoelectric element is considered to be linear and rigid. The mechanical interface between the slider and the counter-mass is specified as a linear spring constant k and a linear damping c . Assuming no contact friction between the counter-mass and the guide surface, there is only one friction between the slider and the guide surface. The contact friction is also considered to be Coulomb friction with the coefficient μ . x_1 , x_2 , l represent the displacement of the slider, the counter-mass and the piezoelectric element respectively; M and m are the mass of the slider and the counter-mass.

In a more general case, external forces act on the slider and the counter-mass (frictional force, magnetic clamping force, etc.), the mass-damper-spring model for the system turns into

$$\begin{cases} M\ddot{x}_1 + c(\dot{x}_1 + \dot{l} - \dot{x}_2) + k(x_1 + l - x_2) = F_1 \\ m\ddot{x}_2 + c(\dot{x}_2 - \dot{l} - \dot{x}_1) + k(x_2 - l - x_1) = F_2 \end{cases} \quad (2-5)$$

where F_1 and F_2 represent the external force on the slider and the counter-mass respectively. By taking the Laplace transform for both sides of above equations, we have

$$(Ms^2 + cs + k)X_1(s) - (cs + k)X_2(s) = -(cs + k)L(s) + F_1(s) + M(sx_1(0) + \dot{x}_1(0)) + c(x_1(0) - x_2(0)) + l(0)$$

$$-(cs + k)X_1(s) + (ms^2 + cs + k)X_2(s) = (cs + k)L(s) + F_2(s) + m(sx_2(0) + \dot{x}_2(0)) + c(x_2(0) - x_1(0)) - l(0)$$

The above algebraic equations can be solved as

$$\begin{bmatrix} X_1 \\ X_2 \end{bmatrix} = \frac{1}{s^2(Mms^2 + c(M+m)s + k(M+m))} \cdot \begin{bmatrix} ms^2 + cs + k & cs + k \\ cs + k & Ms^2 + cs + k \end{bmatrix} \begin{bmatrix} -(cs + k)L + F_1 + I_1 \\ (cs + k)L + F_2 + I_2 \end{bmatrix}$$

Where $I_1 = Mx_1(0)s + I_{10}$ and $I_2 = mx_2(0)s + I_{20}$ represents the terms which contain the initial conditions of the system. We can rewrite the vector $[X_1 \ X_2]^T$ composed of 5 separated vectors.

$$\begin{bmatrix} X_1 \\ X_2 \end{bmatrix} = \begin{bmatrix} X_{1,L} \\ X_{2,L} \end{bmatrix} + \begin{bmatrix} X_{1,F1} \\ X_{2,F1} \end{bmatrix} + \begin{bmatrix} X_{1,F2} \\ X_{2,F2} \end{bmatrix} + \begin{bmatrix} X_{1,I1} \\ X_{2,I1} \end{bmatrix} + \begin{bmatrix} X_{1,I2} \\ X_{2,I2} \end{bmatrix}$$

Where subscript L , $F1$ and $F2$ represent the effect of piezoelectric element, external forces act on the slider and the counter-mass. $I1$ and $I2$ represent the effect of the initial conditions of the system. The individual quantity can be obtained as follows.

$$\begin{cases} X_{1,L} = \frac{-m(cs+k) \cdot L(s)}{Mms^2 + c(M+m)s + k(M+m)} = G_{L1}(s)L(s) \\ X_{2,L} = \frac{M(cs+k) \cdot L(s)}{Mms^2 + c(M+m)s + k(M+m)} = G_{L2}(s)L(s) \end{cases}$$

$$\begin{cases} X_{1,F1} = \frac{(ms^2 + cs + k) \cdot F_1(s)}{s^2(Mms^2 + c(M+m)s + k(M+m))} = G_{F11}(s)F_1(s) \\ X_{2,F1} = \frac{(cs+k) \cdot F_1(s)}{s^2(Mms^2 + c(M+m)s + k(M+m))} = G_{F12}(s)F_1(s) \end{cases}$$

$$\begin{cases} X_{1,F2} = \frac{(cs+k) \cdot F_2(s)}{s^2(Mms^2 + c(M+m)s + k(M+m))} = G_{F21}(s)F_2(s) \\ X_{2,F2} = \frac{(Ms^2 + cs + k) \cdot F_2(s)}{s^2(Mms^2 + c(M+m)s + k(M+m))} = G_{F22}(s)F_2(s) \end{cases}$$

$$\begin{cases} X_{1,I1} = \frac{(ms^2 + cs + k) \cdot (Mx_1(0)s + I_{10})}{s^2(Mms^2 + c(M+m)s + k(M+m))} \\ X_{2,I1} = \frac{(cs+k) \cdot (Mx_1(0)s + I_{10})}{s^2(Mms^2 + c(M+m)s + k(M+m))} \end{cases}$$

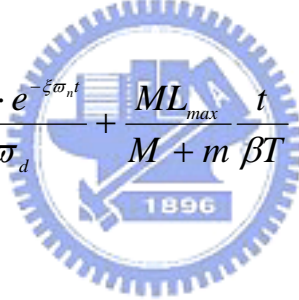
$$\begin{cases} X_{1,I2} = \frac{(cs+k) \cdot (mx_2(0)s + I_{20})}{s^2(Mms^2 + c(M+m)s + k(M+m))} \\ X_{2,I2} = \frac{(Ms^2 + cs + k) \cdot (mx_2(0)s + I_{20})}{s^2(Mms^2 + c(M+m)s + k(M+m))} \end{cases}$$

By the inverse Laplace transform $L^{-1}\{\cdot\}$ the displacement of the slider under actuation of IDM can be obtained as

$$x_1(t) = L^{-1}\{G_{L1}(s)L(s)\} + L^{-1}\{G_{F11}(s)F_1(s)\} + L^{-1}\{G_{F21}(s)F_2(s)\} \\ + L^{-1}\{X_{1,I1}(s)\} + L^{-1}\{X_{2,I2}(s)\}$$

In the following formulations, we assume the load capacity of piezoelectric element is large enough and the output is corresponding to the rapid deflection stage or the slow deflection stage of the piezoelectric element only. The displacement of slider drive previously can be rewritten as

$$x_{1,L} = \frac{mL_{max} \sin \varpi_d t \cdot e^{-\xi \varpi_n t}}{\beta T (M + m) \varpi_d} - \frac{mL_{max}}{M + m} \frac{t}{\beta T}$$

$$x_{2,L} = \frac{-ML_{max} \sin \varpi_d t \cdot e^{-\xi \varpi_n t}}{\beta T (M + m) \varpi_d} + \frac{ML_{max}}{M + m} \frac{t}{\beta T}$$


where β represents the percentage of the slanting stage in a cycle (γ or $1-\gamma$); L_{max} represents the maximum deflection of the piezoelectric element; γ and T depicted in Figure 2.7 are the complement duty cycle and the period of triangular waveform respectively. Similarly, we can obtain the relation between the displacement of the slider and external constant forces F_1 and F_2 as follows.

$$x_{1,F1}(t) = \left\{ \left[\frac{-cm \sin \varpi_d t}{2kM(M+m)\varpi_d} - \frac{m^2 \cos \varpi_d t}{k(M+m)^2} \right] \cdot e^{-\xi \varpi_n t} + \frac{m^2}{k(M+m)^2} + \frac{t^2}{2(M+m)} \right\} F_1$$

$$x_{2,F1}(t) = \left\{ \left[\frac{c \sin \varpi_d t}{2k(M+m)\varpi_d} + \frac{Mm \cos \varpi_d t}{k(M+m)^2} \right] \cdot e^{-\xi \varpi_n t} - \frac{Mm}{k(M+m)^2} + \frac{t^2}{2(M+m)} \right\} F_1$$

$$x_{1,F2}(t) = \left\{ \left[\frac{c \sin \varpi_d t}{2k(M+m)\varpi_d} + \frac{Mm \cos \varpi_d t}{k(M+m)^2} \right] \cdot e^{-\xi \varpi_n t} - \frac{Mm}{k(M+m)^2} + \frac{t^2}{2(M+m)} \right\} F_2$$

$$x_{2,F2}(t) = \left\{ \left[\frac{-Mc \sin \varpi_d t}{2km(M+m)\varpi_d} - \frac{M^2 \cos \varpi_d t}{k(M+m)^2} \right] \cdot e^{-\xi \varpi_n t} + \frac{M^2}{k(M+m)^2} + \frac{t^2}{2(M+m)} \right\} F_2$$

Finally, the initial condition of slider displacement and counter-mass displacement for each stage are

$$x_{1,I1}(t) = \left[\frac{2mI_{10} - c(M+m)x_1(0)}{2M(M+m)\varpi_d} \sin \varpi_d t + \frac{mx_1(0)}{M+m} \cos \varpi_d t \right] e^{-\xi \varpi_n t} + \frac{Mx_1(0) + I_{10}t}{M+m}$$

$$x_{2,I1}(t) = \left[\frac{c(M+m)x_1(0) - 2mI_{10}}{2m(M+m)\varpi_d} \sin \varpi_d t - \frac{Mx_1(0)}{M+m} \cos \varpi_d t \right] e^{-\xi \varpi_n t} + \frac{Mx_1(0) + I_{10}t}{M+m}$$

$$x_{1,I2}(t) = \left[\frac{c(M+m)x_2(0) - 2MI_{20}}{2M(M+m)\varpi_d} \sin \varpi_d t - \frac{mx_2(0)}{M+m} \cos \varpi_d t \right] e^{-\xi \varpi_n t} + \frac{mx_2(0) + I_{20}t}{M+m}$$

$$x_{2,I2}(t) = \left[\frac{2MI_{20} - c(M+m)x_2(0)}{2m(M+m)\varpi_d} \sin \varpi_d t + \frac{Mx_2(0)}{M+m} \cos \varpi_d t \right] e^{-\xi \varpi_n t} + \frac{mx_2(0) + I_{20}t}{M+m}$$

From above formulation, we can conclude the characteristic of IDM as a second order dynamic system with damped natural frequency and damping

ratio as follows.

$$\omega_d = \omega_n \sqrt{1 - \xi^2} = \frac{1}{2Mm} \sqrt{(M + m)[4kMm - c^2(M + m)]} \quad (2-6)$$

$$\xi \omega_n = \frac{c(M + m)}{2Mm} \quad (2-7)$$

$$\xi = \frac{c(M + m)}{\sqrt{4kMm(M + m)}} = \frac{c}{2} \sqrt{\frac{M + m}{kMm}} \quad (2-8)$$



Chapter 3 Experiment

3.1 Improvement of IDM

Figure 3.1 and Figure 3.2 illustrate the previous and advanced structure of IDM. The disadvantage of previous one is that the counter-mass will vibrate up and down which may change the normal force of the slider when the piezoelectric element deforms rapidly. The behavior affects the contact friction between the slider and the guide surface and enormously increases the complexity of the system because frictional force is one of the important points. The vibration also causes inaccuracy in measuring. Now, a new concept of IDM is constructed to solve the problem. In the advanced structure of IDM, piezoelectric elements are fixed from end to end of the slider and the counter-mass. Oilless bearings are placed across the intermediate mechanism to prevent the piezoelectric element from vibration and reduce the friction between piezoelectric elements and the intermediate mechanism during deformation. Besides, the guide is used to yield IDM to walk step by step straightly.

As shown in Figure 3.3, P-840.10 preloaded LVPZT translators, used in IDM for experiment, are high resolution linear actuators for static and dynamic applications. They provide sub-millisecond response and sub-nanometer resolution. These translators are equipped with highly reliable multilayer PZT ceramic stacks protected by a non-magnetic stainless steel case with internal spring preload that makes them ideal for dynamic applications. The standard translator tip and base have tapped holes. Technical

notes are listed in Table 3.1.

3.2 Experimental Setup

Figure 3.4 and Figure 3.5 depict the overall structure and configuration with actual instrument for measuring the displacement of the piezoelectric actuator respectively. The photographs of the system and IDM are also presented in Figure 3.6 and Figure 3.7. In the experiment, the HP10705A interferometer with 10nm (0.4 μ in) resolution and 3MHz maximum data update rate measures the actual output displacement of IDM. The sampling time of the data is controlled by DSP module and then sent to HP10885A. The HP10885A Axis board's primary function is to convert reference and measurement signals from an HP 5517C laser head and measurement receiver to a 32-bit digital position word. The unit of measurement associated with the position word is a fraction of the wavelength of the laser light being used. A conversion is required if the position must be known in some other units (mm, inch, etc.).

After conversion, the raw data is read by DSP module directly. The main functions of the DSP module are:

- (1) to send signals to HP10885A to control the sequence of data sample and hold (8 bits digital output);
- (2) to do data reading (32 bits digital input);
- (3) to produce driving voltage waveforms needed in the experiment (8 bits DA) and send to IDM.

We achieve this goal by utilizing code composer studio (CCS) software

to integrate these tasks into a program which can be loaded to the DSP controller. Because of low driving voltage waveforms from DSP module (8 bits DA), a voltage amplifier is needed to amplify the analog signal from 0~2V to 0~100V to drive the piezoelectric actuator.

3.3 DSP Program Flowchart

The 2407A DSP controllers shown in figure 3.8 are designed to meet the needs of control-based applications. By integrating the high performance of a DSP core and the on-chip peripherals of a microcontroller into a single-chip solution, the 240xA series yields a device that is an affordable alternative to traditional microcontroller units (MCUs) and expensive multichip designs. At 40 million instructions per second (MIPS), the 2407A DSP controllers offer significant performance over traditional 16-bit microcontrollers and microprocessors. The 16-bit, low power, fixed-point DSP core of the 2407A device provides analog designers a digital solution that does not sacrifice the precision and performance of their systems. See details in Figure 3.9 and Figure 3.10.

Code composer studio (CCS) is a fully software integrated development environment (IDE) for building and debugging programs for the DSK (DSP Starter Kit), i.e. the DSP board. CCS integrates all host and target tools in a unified environment to simplify DSP system configuration and application design. This easy to use development environment allows DSP designers of all experience levels full access to all phases of the code development process. The software is used for three phases in the overall DSP system design

process:

(1) Coding and building: writing code using the editor, creating a 'project', and compiling and linking.

(2) Debugging: syntax checking, probe points, break points

(3) Analysis: statistics, benchmarking, real-time debugging

Figure 3.11 describes the complete flowchart of the DSP program. The processes are as follows:

(1) Start: The program starts.

(2) CPU will be initialized first. Then we set and enable time interrupt to define the sampling time.

(3) A while loop for DA control waveforms applying to the piezoelectric actuator is executed. The program waits for the time interrupt every 50 us (sampling rate = 20kHz).

(4) The program gets into time interrupt, the DSP module starts to read data by 32bits digital input.

(5) MSB Check: Because we do not know if an error occurs, the received data has to be checked first if an error occurs. The method provided from operating manual is to examine the most significant bit (MSB). If the MSB is one (true), it implies the data is correct. Otherwise, there exists an error. We should adjust all the experiments of the laser interferometer and see if the light status is ready especially the indicator of the receiver. Then restart the program again to step (1).

(6) Sign Check: The meaning of the second MSB indicates the sign of the position value; therefore it is sometimes called the sign bit. The sign bit zero (false) means positive and one (true) means negative position. Negative position needs to be calculated by 2's complement. The position register is

saved to the buffer.

(7) End: The program ends.

(8) Measurement: After the program ends, the position register saved in the buffer can be transferred to the real world displacement. The following equation describes how position is calculated from the value in the position register:

$$Position = Position\ register \times \frac{\lambda}{N} \times Compensation\ number$$

where:

$\lambda = 632.99135$ nanometers (for HP5517C)

$N = 64$ when linear optics are being used

$N = 128$ when plane mirror optics are being used

$N = 256$ when high resolution optics are being used

$$Compensation\ number = \frac{1}{Air's\ index\ of\ refraction} = 0.9997288$$

Then the experimental results will be plotted into a time-position graph step by step continuously. These files can help us to compare the results of different driving waveforms.

3.4 Experimental Results

Figure 3.12 to Figure 3.15 shows the displacement of the counter-mass with 100V, 95% duty triangle input waveforms but different frequencies. During the rapid phase of the input waveform, the position of the counter-mass suddenly drops to a bottom because the piezoelectric actuator contracts. The slider makes a big displacement at this point according to the

principle of the stick-slip device and the counter-mass follows the step, too. The vibration of the slider caused by preload spring will continue little time when the slow phase of the input waveform is applying to the piezoelectric actuator. Thus, the position of the counter-mass linked to the slider will follow the reaction. At lower frequency, the position of the counter-mass becomes steady with the slow phase of the input waveform. As the frequency of input waveform increases, the effect takes place obviously. Steady rise of the position no longer exists.

The positioning of the mechanism we emphasize is on the slider. Take a look at Figure 3.16 to 3.19. These figures illustrate the displacement of the slider with 100V, 95% duty triangle input waveforms but different frequencies. The slider steps a little displacement at first resulting from the slow extension of the piezoelectric actuator. With the turning point of the input waveform, the piezoelectric actuator tends to return to the original length. Due to the rapid phase process, the piezoelectric actuator contracts so fast that the inertial force greatly exceeds the friction force and the slider starts to move. The internal spring preload of the piezoelectric actuator will make a mechanical vibration during the fast contraction, thus the slider accompanies the effect to converge to a steady state finally. One step is finished. By the operating cycle, IDM can walk step by step periodically.

Some problems about the frequency of the input waveform exist. If the frequency becomes higher, the convergence of every one step becomes worse because of the mechanical vibration of IDM. This brings about the difficulty of precise positioning. Therefore we should avoid using unreasonable frequency exceeding 500Hz.

100Hz, 95% duty triangle driving waveform is chosen as the standard of

positioning in the experiment due to the better stepping. Figure 3.20 and Figure 3.21 depicts the mean value of step of the slider and the counter-mass respectively. Each step is about 1 μ m.

The forward movement of IDM with different input voltages is shown in Figure 3.22. It is easy to see that the step size increases as the input voltage increases since higher input voltage causes stronger inertial force to make a step. Conversely, IDM can also do the backward movement as introduced in section 2.4 while we change the duty of the triangle waveform. The measurement of the backward movement is shown in Figure 3.23.

3.5 Observation of Forward and Backward Movement

Figure 3.24 and Figure 3.25 plots the displacement of the slider with input frequency 100Hz but different amplitudes and duties. The step size increases obviously as the input voltage increases. It also depends on the duty of the input waveform. An extreme duty is selected to make a larger displacement due to the sudden inertial force is larger to overcome the friction force.

The forward movement of IDM is similar to the backward movement but little difference in step size. With same condition but converse duty, the step of the backward movement is larger than that of the forward movement. One possibility is to assume the friction between the bottom of IDM and the surface of the guide in forward and backward is quite different since the inaccurate manufacture of IDM. Another possibility may be the sudden stop of the principles of IDM illustrated in Figure 2.4. The difference between forward and backward movement results from the sudden stop of the

counter-mass which contributes to the displacement in the same direction or not.

3.6 Discovery of IDM

From several experiments, we found that the standard sine waveform during certain frequencies may let IDM move. It is surprised to break the normal convention of applying the asymmetric waveforms to drive IDM. We just need general sine waveform with certain frequency (about 1300Hz to 1600Hz) and lower voltage to drive IDM. The phenomenon may help us to do longer traveling. Figure 3.26 is a good example of movement by 50V, 1400Hz sine waveform input. Figure 3.27 depicts the velocity of the slider with various sine waveforms. IDM do not move anymore out of the range of the frequency.

With sine waveform input voltage higher than 60V in the range of frequency, the displacement of IDM quickly moves beyond the sensing range of the laser interferometer. We can not handle the displacement of IDM anymore by interferometer measuring system. The scene of walking even can be seen with a naked eye. Therefore, larger displacement positioning (mm, cm, etc.) is not the question as long as the characteristic is known well.

Chapter 4 Conclusion

In this research, the impact drive mechanism (IDM), a simple but effective device, is realized experimentally to perform the precise positioning. The forward and backward movement of IDM is the same as our expectation. It will walk step by step periodically with appropriate amplitude, frequency and duty of the triangle input waveform. These results lead to the conclusions in brief.

(1)The step size of movement increases as the input voltage increases.

(2)The behavior of movement decays in high frequency operation.

Precise positioning should avoid driving voltage with high frequency.

(3)The input waveform with extreme duty makes the step larger.

(4)The effect of backward movement is better than that of the forward movement.

(5)A short distance is achieved by designing the asymmetric triangle waveforms. The new discovered method can be applied to much longer traveling.

For the moment, we shall confirm our attention to the source of error. There is no disagreement on this point that the hysteresis causes uncertain displacement in positioning. Second, the cable of the piezoelectric actuator greatly affects the movement of IDM. Thus the radius of the cable should be decreased as possible to reduce the external force exerting influence on IDM. Third, the temperature compensation is not well-handled. It is important to remember that such accuracy is obtainable only if the surrounding environment is controlled, since temperature changes and vibration may cause inaccurate measurement in positioning at the nanometer level. Besides, IDM

structure should be carefully manufactured in the best way.

Piezoelectric actuators can be operated in open-loop and closed-loop modes. In open-loop mode, displacement roughly corresponds to the driving voltage. This mode is ideal when the absolute position accuracy is not critical, or when the position is controlled by data provided by an external sensor (interferometer, CCD chip etc.). Open-loop piezoelectric actuators exhibit hysteresis and creep behavior, just like other open-loop positioning systems.

Closed-loop actuators are ideal for applications requiring high linearity, long-term position stability, repeatability and accuracy. A servo-controller (digital or analog) determines the voltage to send to the piezoelectric actuators by comparing a reference signal (commanded position) to the actual position, as reported by the feedback position sensor. This is our target to make efforts in the future.



Reference

- [1] T. Higuchi, Y. Yamagata, K. Furutani & K. Kudoh, "Precise Positioning Mechanism Utilizing Rapid Deformations of Piezoelectric Elements", *Proceedings of the IEEE MEMS Workshop*, 1990, pp.222-226.
- [2] S. Ling, H. Du & T. Jiang, "Analytical and Experimental Study on a Piezoelectric Linear Motor", *Smart Materials and Structures*, Vol.7, No.3, Jun, 1998, pp.382-388.
- [3] K. Furutani, T. Higuchi, Y. Yamagata & N. Mohri, "Effect of Lubrication on Impact Drive Mechanism", *Precision Engineering*, Vol.22, No.2, 1998, pp.78-86.
- [4] J. Mendes, M. Nishimura, K. Tomizawa, Y. Yamagata & T. Higuchi, "Print Board Positioning System Using Impact Drive Mechanism", *Proceedings of the SICE Annual Conference*, Jul, 1996, Tottori, Jpn, pp.1123-1128.
- [5] Y. Wang, M. Mason, "Two-Dimensional Rigid-Body Collisions with Dry Friction", *Transactions of the ASME*, Vol.59, Sep, 1992, pp.635-642.
- [6] M. Kurisu, T. Yoshikawa, "Tracking Control for An Object in Pushing Operation", *Proceedings of the 1996 IEEE/RSJ International Conference on Intelligent Robots and Systems*, Vol.2, Nov, 1996, Osaka, Jpn, pp.729-736.
- [7] H. Alexander, H. Lakhani, "Robotic Control of Sliding Object Motion and Orientation", *Proceedings of the 1996 IEEE/RSJ International Conference on Robotic and Automation*, Apr, 1996, Minneapolis, Minnesota, pp.3336-3342.
- [8] Y. Yamagata, T. Higuchi, "A Micropositioning Device for Precision Automatic Assembly Using Impact Force of Piezoelectric Elements",

Proceedings of IEEE International Conference on Robotics and Automation, May, 1995, Nagoya, Jpn, pp.666-671.

- [9] K. Furutani, N. Mohri & T. Higuchi, “Self-Running Type Electrical Discharge Machine Using Impact Drive Mechanism”, *Proceedings of IEEE/ASME International Conference on Advanced Intelligent Mechatronics*, Jun, 1997, Tokyo, Jpn, pp.88.
- [10] K. Furutani, N. Mohri & T. Higuchi, “Self-Running Type Electrical Discharge Machine Using Impact Drive Mechanism”, *Seimitsu Kogaku Kaishi/Journal of the Japan Society for Precision Engineering*, Vol.63, No.9, Sep, 1997, pp.1290-1294.
- [11] K. Ikuta, S. Aritomi & T. Kabashima, “Tiny Silent Linear Cybernetic Actuator Driven by Piezoelectric Device with Electromagnetic Clamp”, *Proceedings of the IEEE Micro Electro Mechanical Systems Workshop*, Feb, 1992, Travemuende, Ger, pp.232-237.
- [12] T. Idogaki, H. Kanayama, N. Ohya, H. Suzuki & T. Hattori, “Characteristics of the Piezoelectric Locomotive Mechanism for an In-Pipe Micro Inspection Machine”, *Proceeding of the International Symposium on Micro Machine and Human Science*, Oct, 1995, Nagoya, Jpn, pp.193-198.
- [13] T.L. Jordan & Z. Ounaies, “Piezoelectric Ceramics Characterization”, *ICASE Report*, No.2001-28, Sep, 2001.
- [14] 鄭仲哲,「利用壓電致動器之精密定位」,國立交通大學,博士論文,民國 92 年。
- [15] 林容益, DSP/CPLD控制技術及應用, 初版, 全華出版社, 台北, 民

國 90 年。

[16] 新華電腦，DSP從此輕鬆跑 (TI DSP 320LF2407A)，初版，台科大圖

書股份有限公司，台北，民國 92 年。



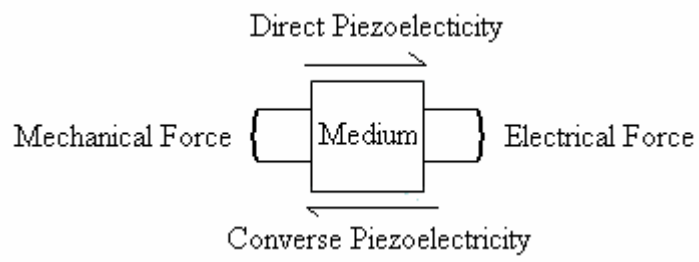


Figure 1.1 Piezoelectric effect and its reversibility

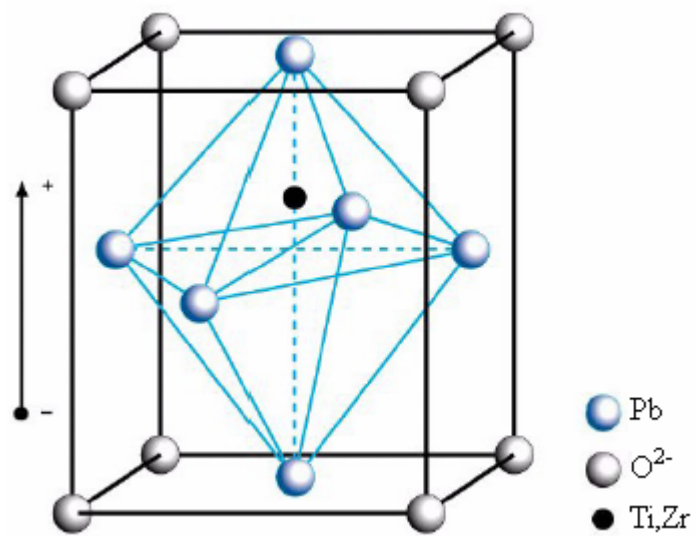


Figure 1.2 Perovskite structure

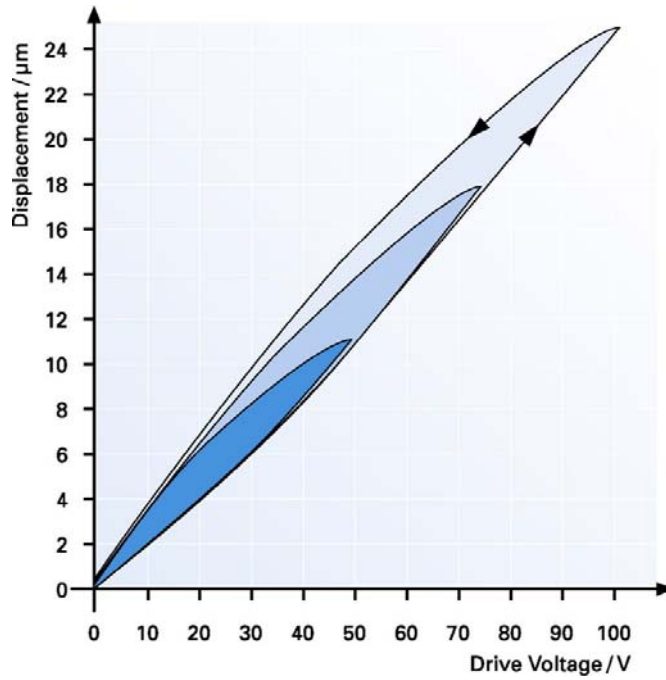


Figure 2.1 Hysteresis curves of an open loop piezoelectric actuator

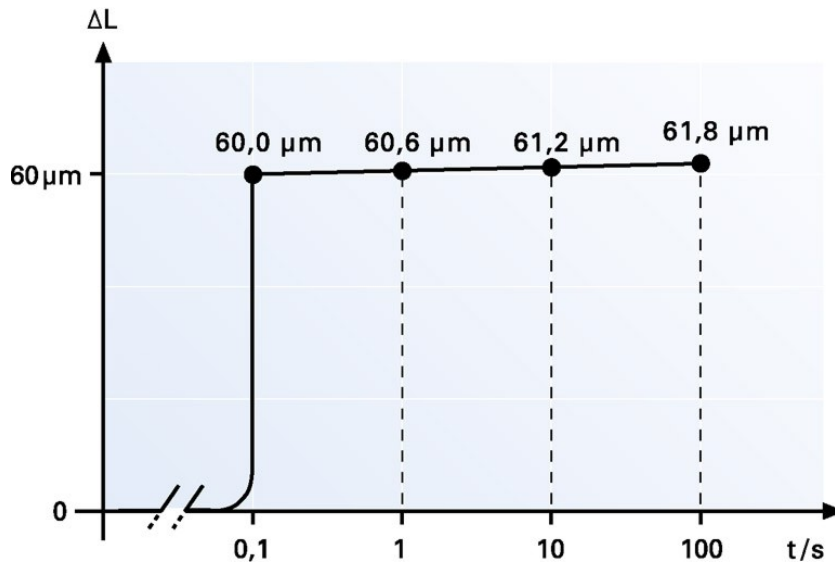


Figure 2.2 Creep of an open loop piezoelectric actuator

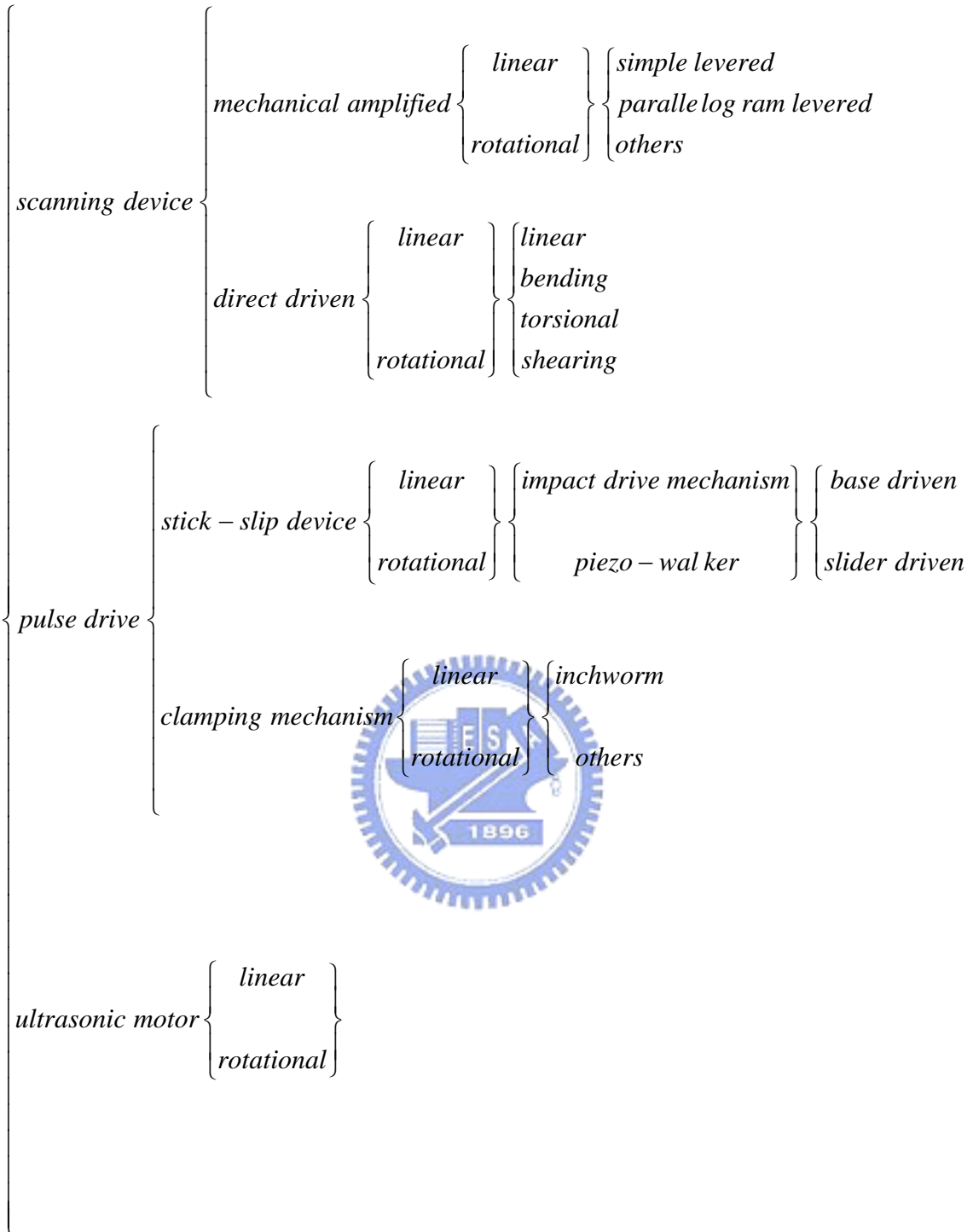
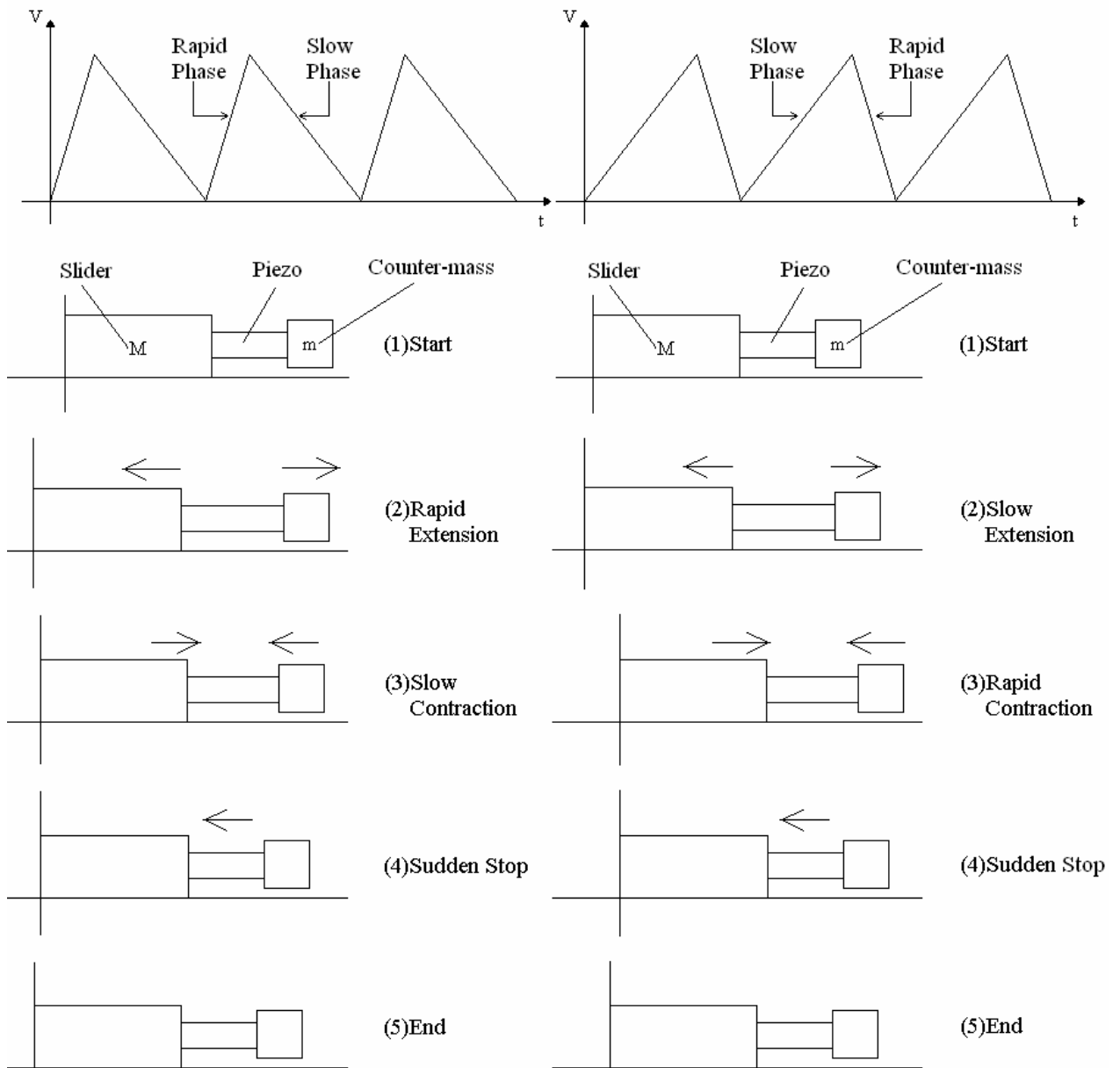


Figure 2.3 Classification of piezoelectric positioning device



(a)5% duty input: backward movement (b)95% duty input: forward movement

Figure 2.4 Operating principle of IDM

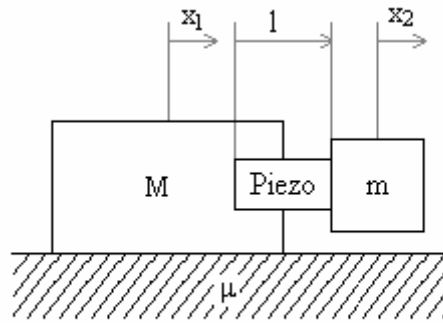


Figure 2.5 The rigid body of model of IDM

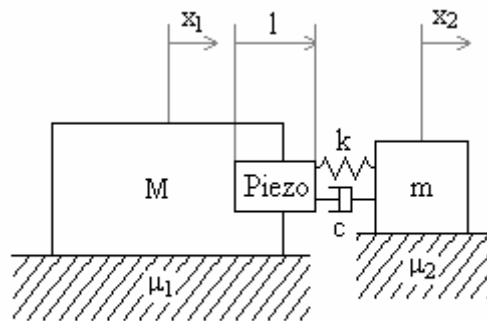


Figure 2.6 The mass-damper-spring model of IDM

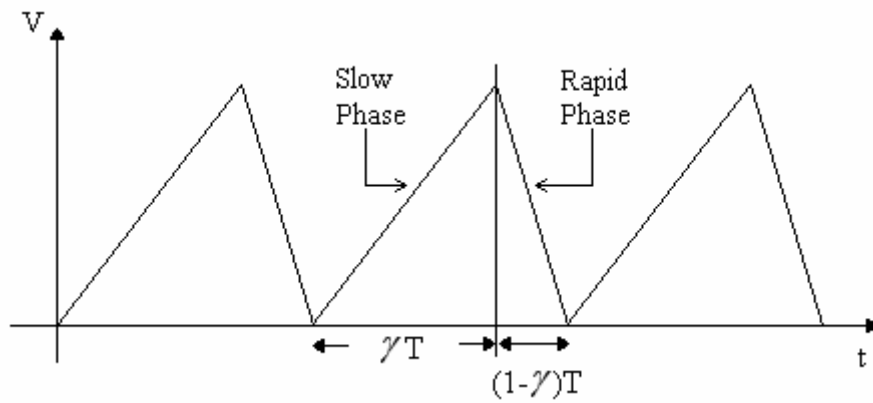


Figure 2.7 The typical input pattern for IDM

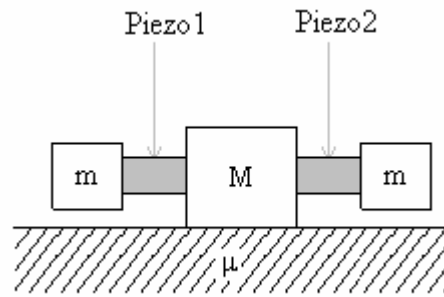


Figure 3.1 Previous IDM structure

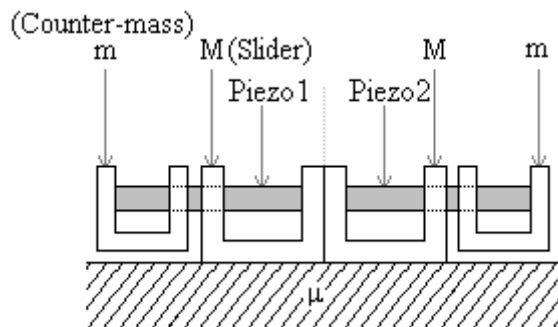


Figure 3.2 Advanced IDM structure

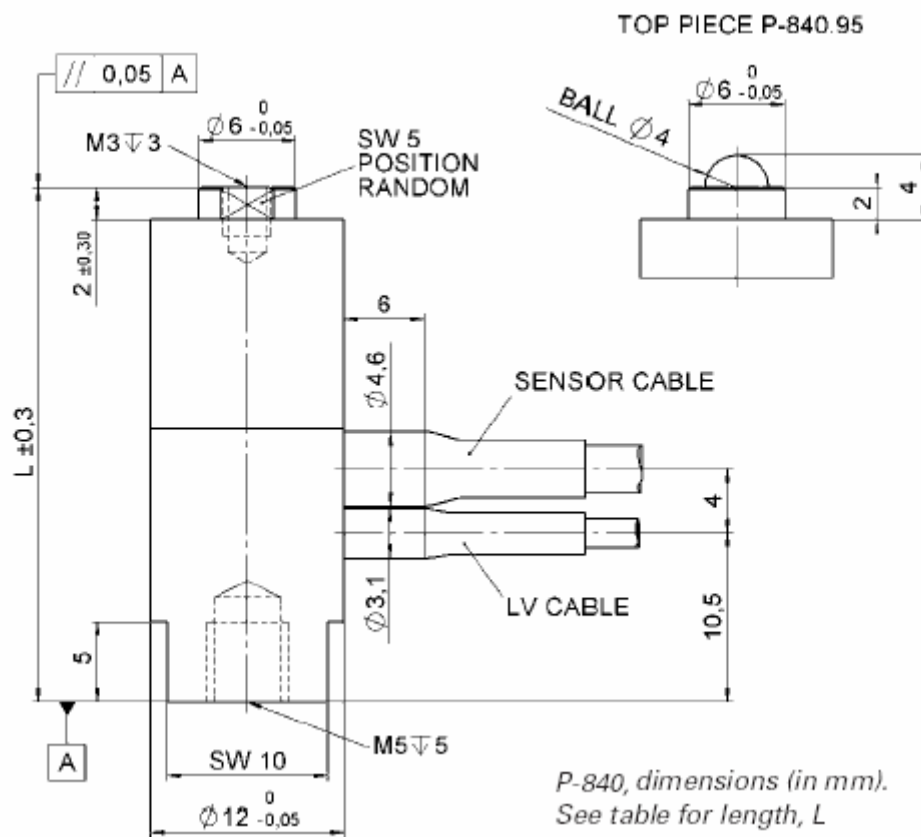


Figure 3.3 P-840.10 preloaded LVPZT translator

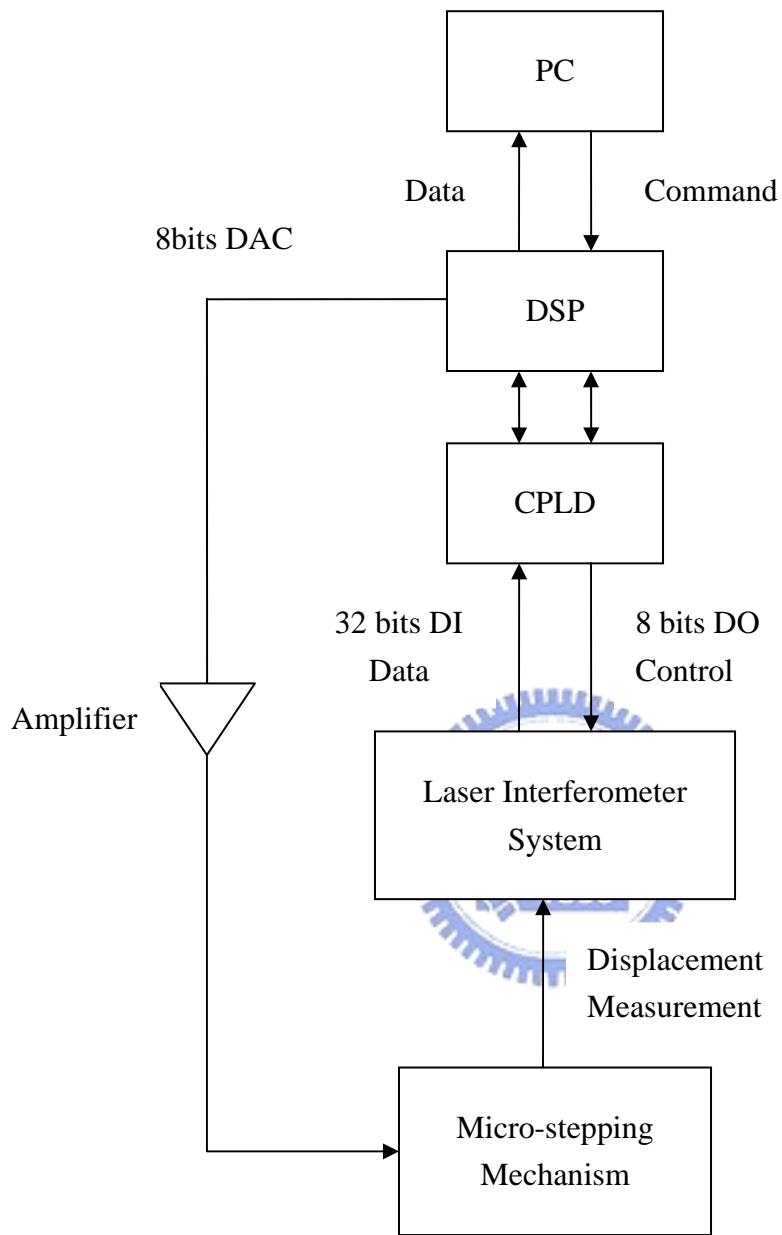


Figure 3.4 Structure for measurement

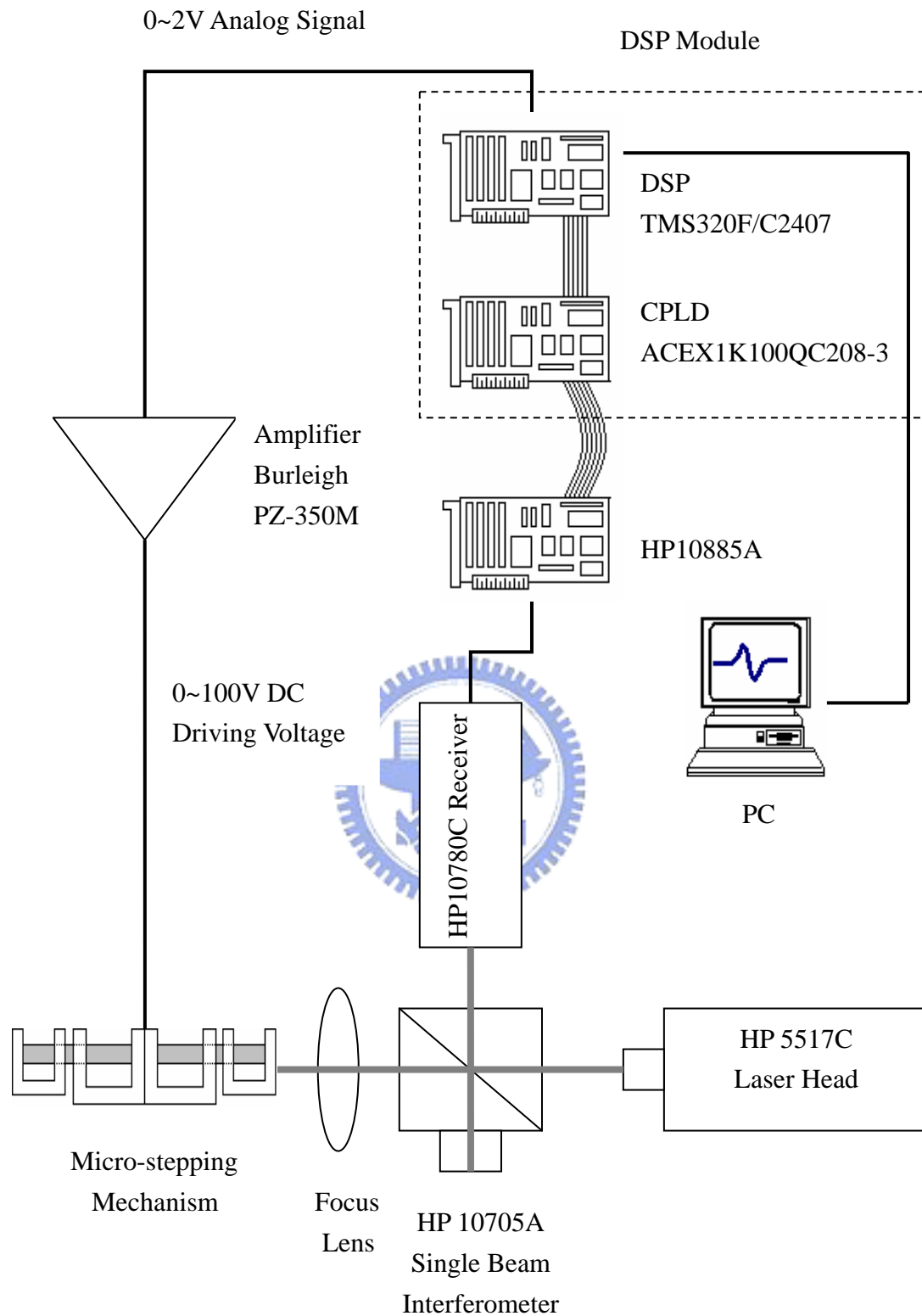


Figure 3.5 System configuration

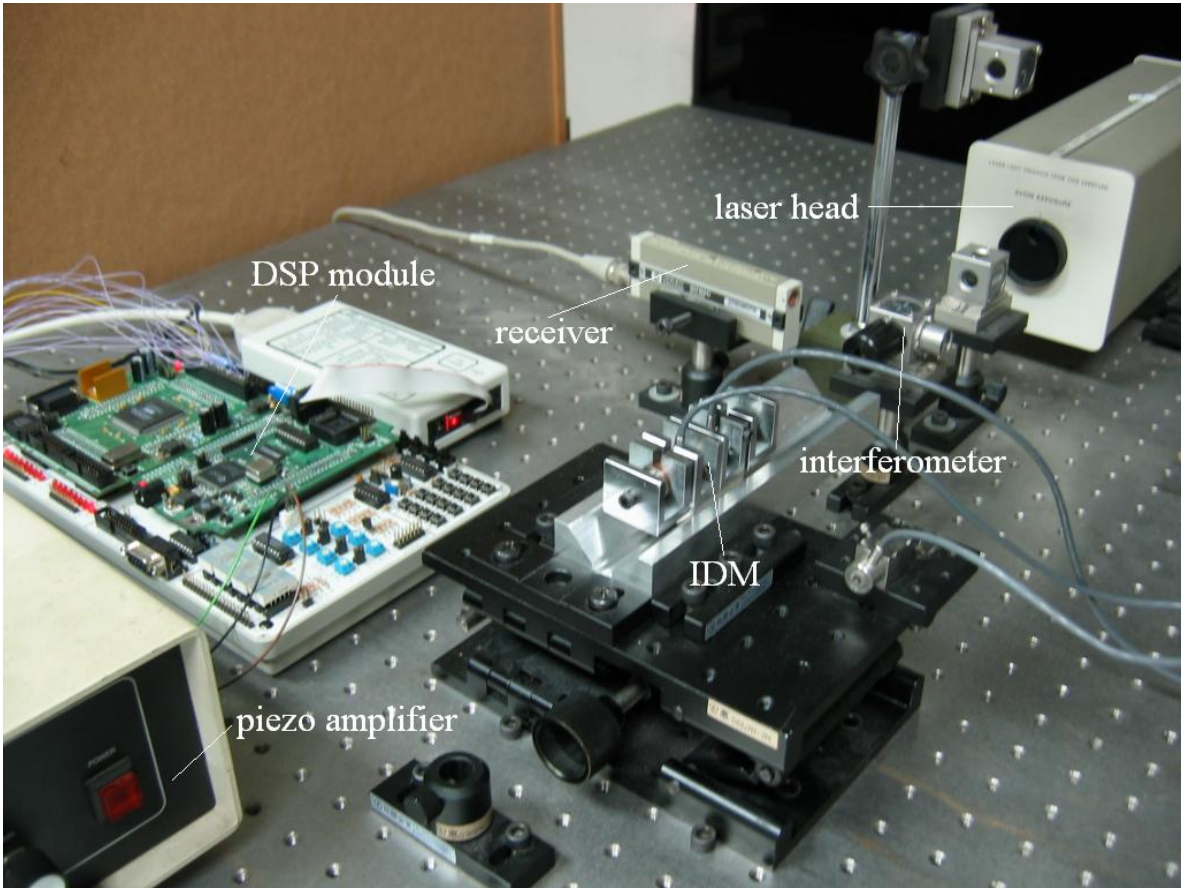


Figure 3.6 Experiment setup

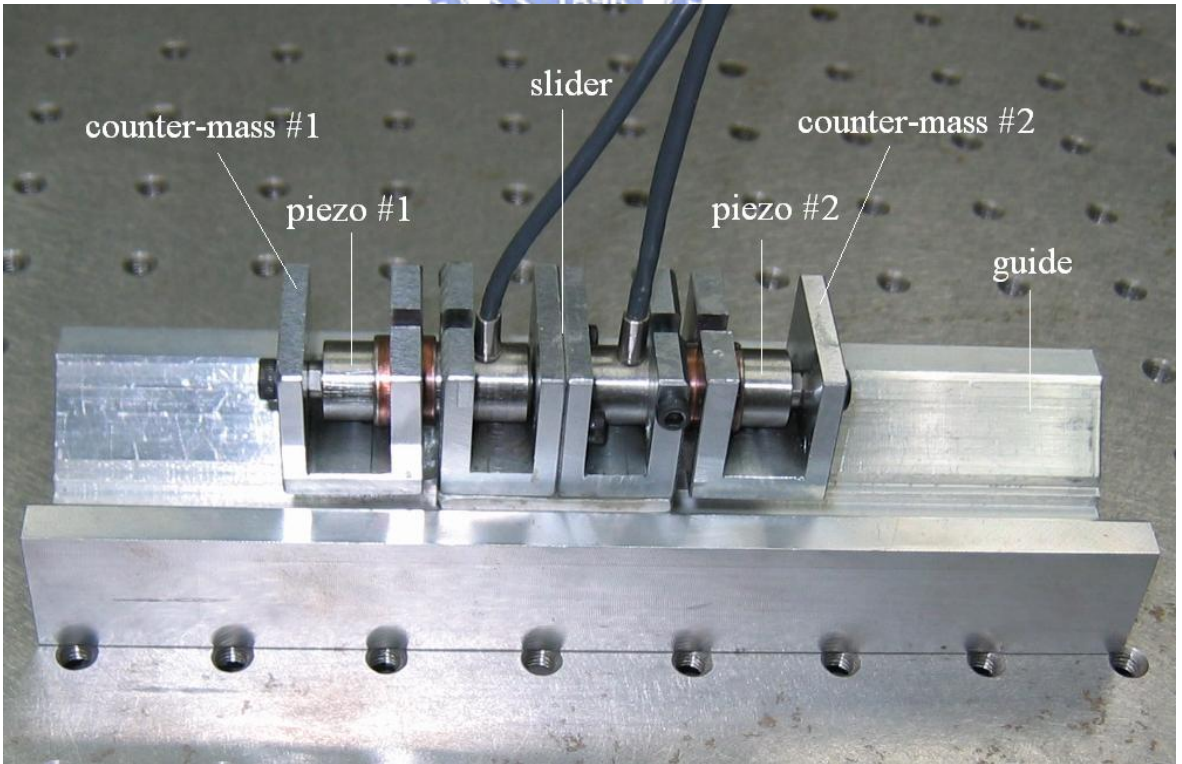


Figure 3.7 Impact drive mechanism

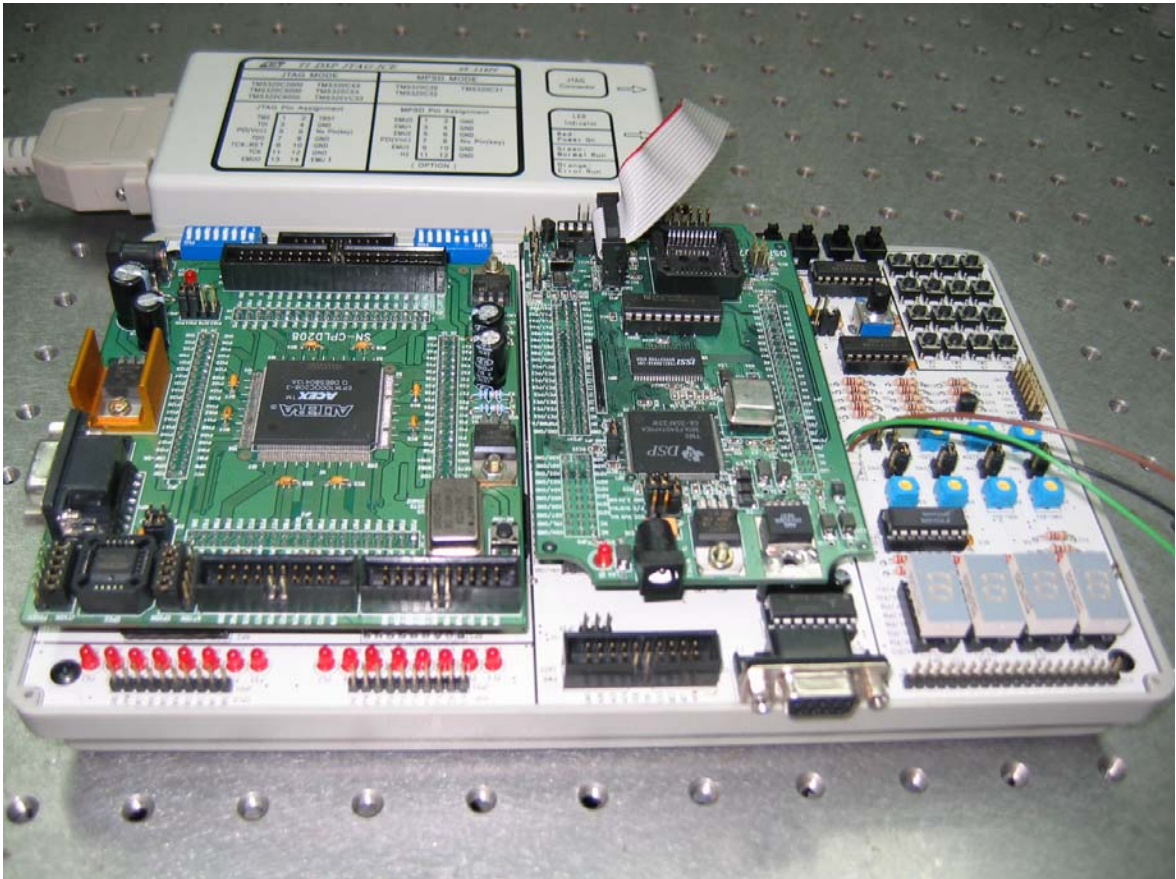


Figure 3.8 DSP module

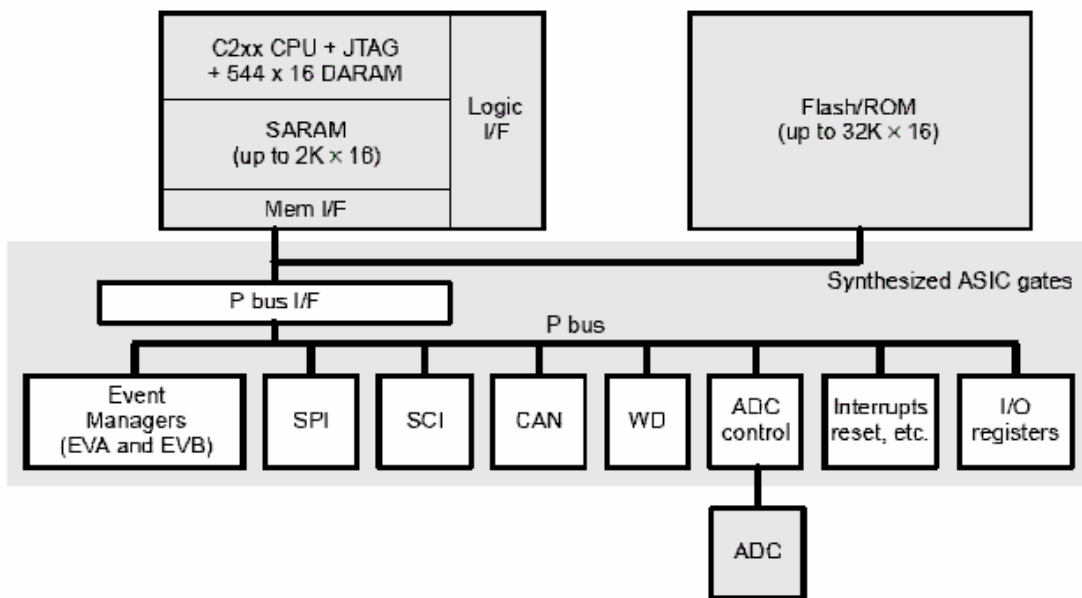


Figure 3.9 2407A device architecture

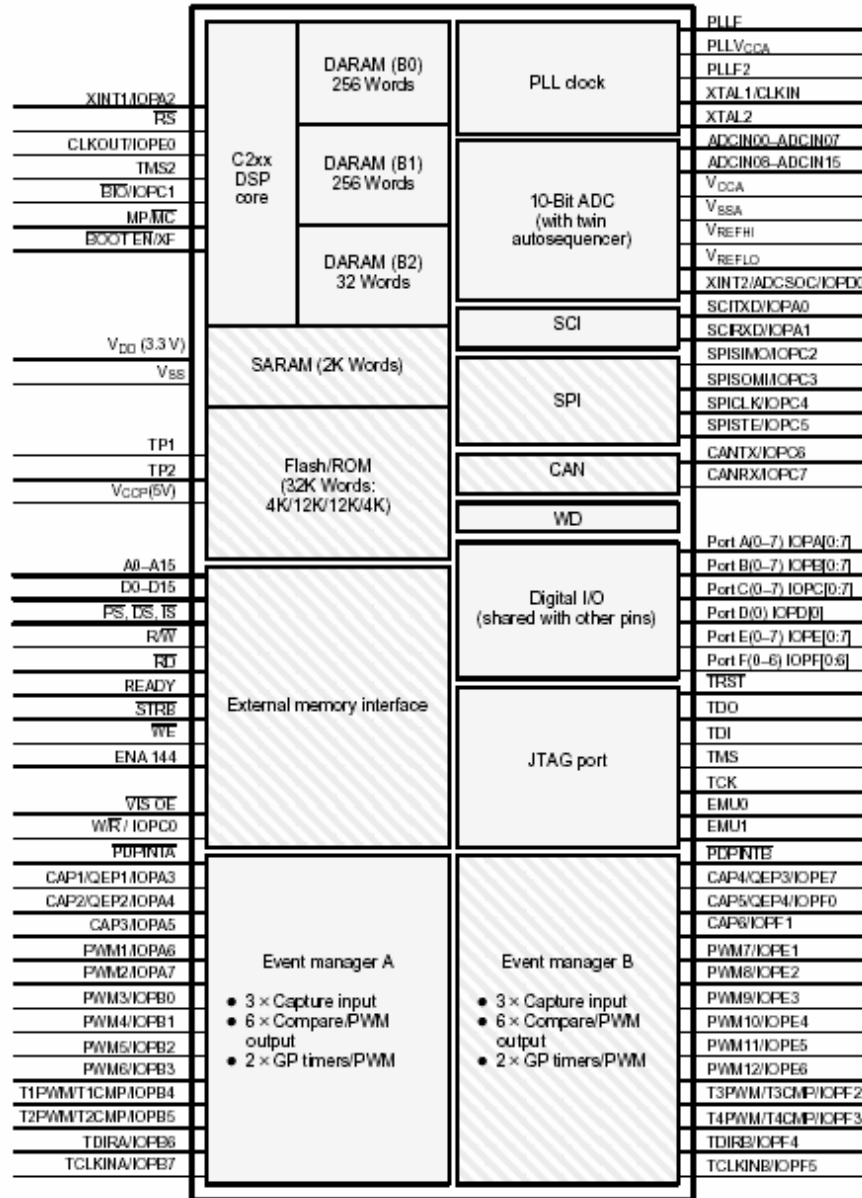


Figure 3.10 Functional block diagram of the 2407A DSP controller

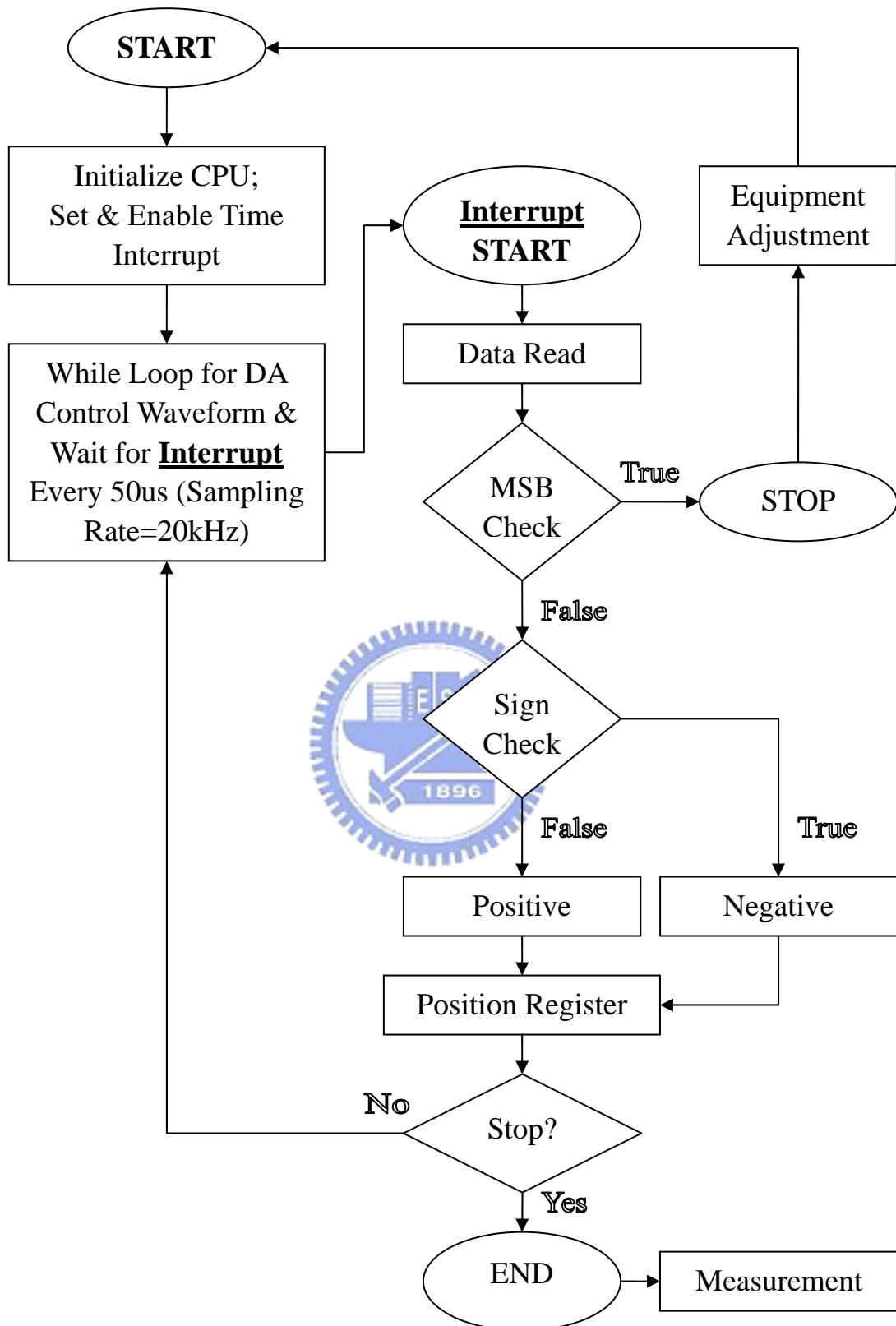


Figure 3.11 Program flow

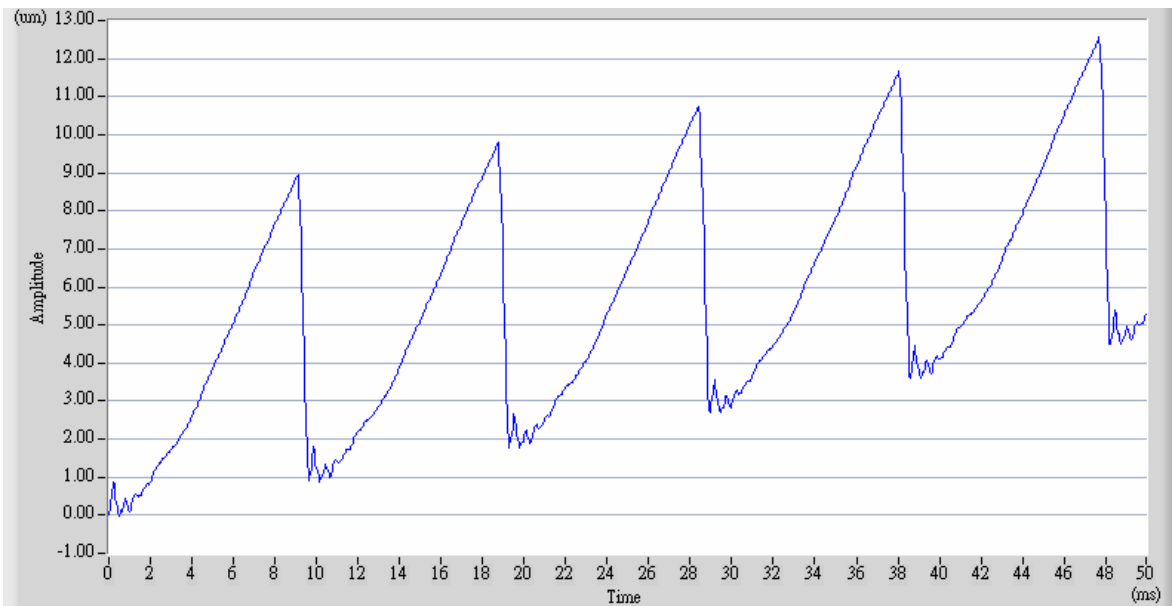


Figure 3.12 100V, 100Hz, 95% duty input, displacement of the counter-mass

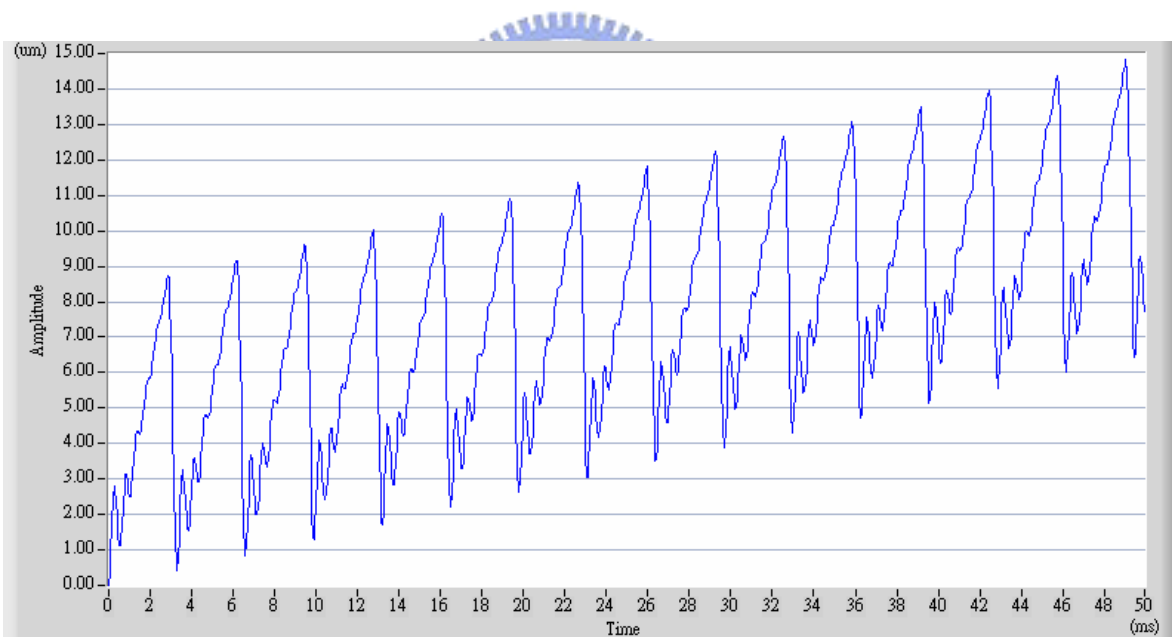


Figure 3.13 100V, 300Hz, 95% duty input, displacement of the counter-mass

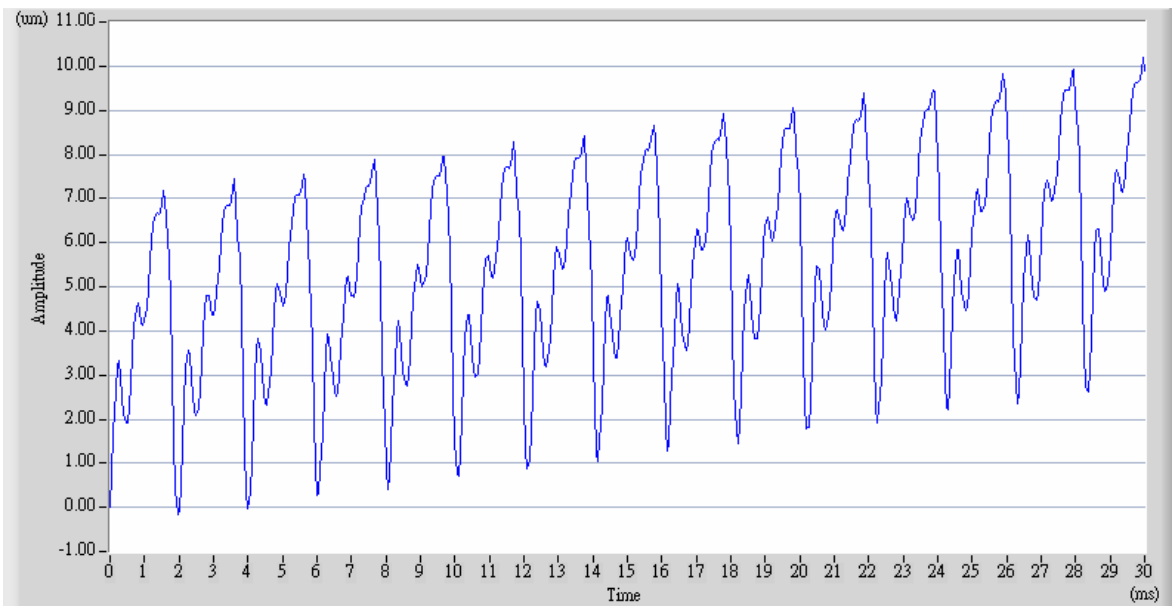


Figure 3.14 100V, 500Hz, 95% duty input, displacement of the counter-mass

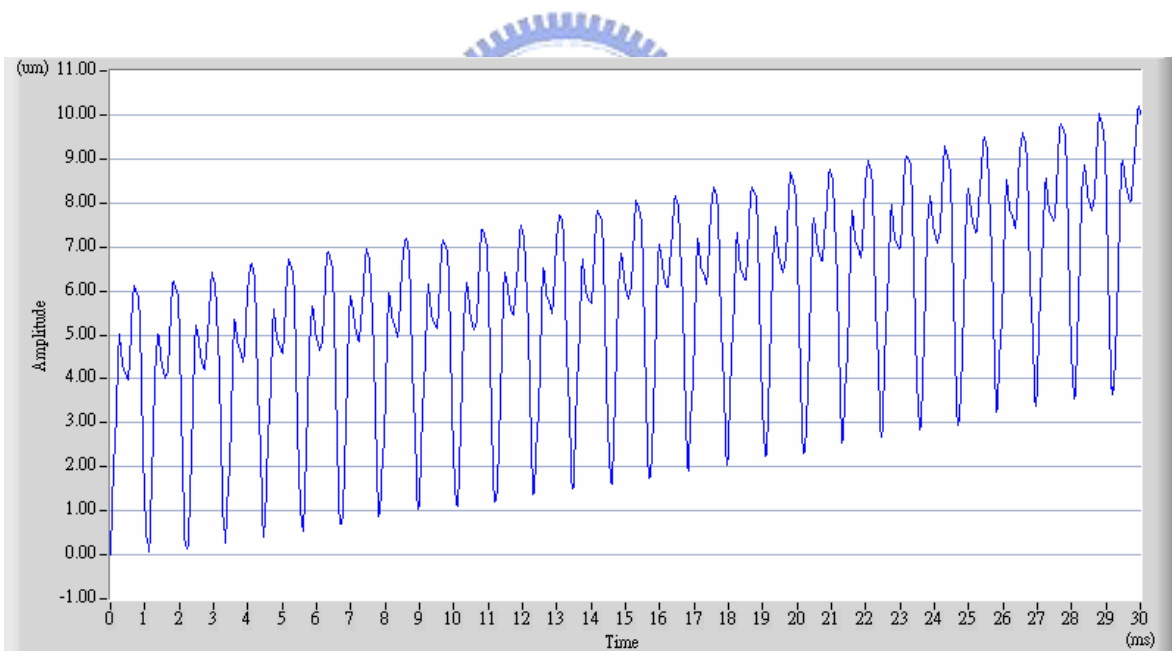


Figure 3.15 100V, 900Hz, 95% duty input, displacement of the counter-mass

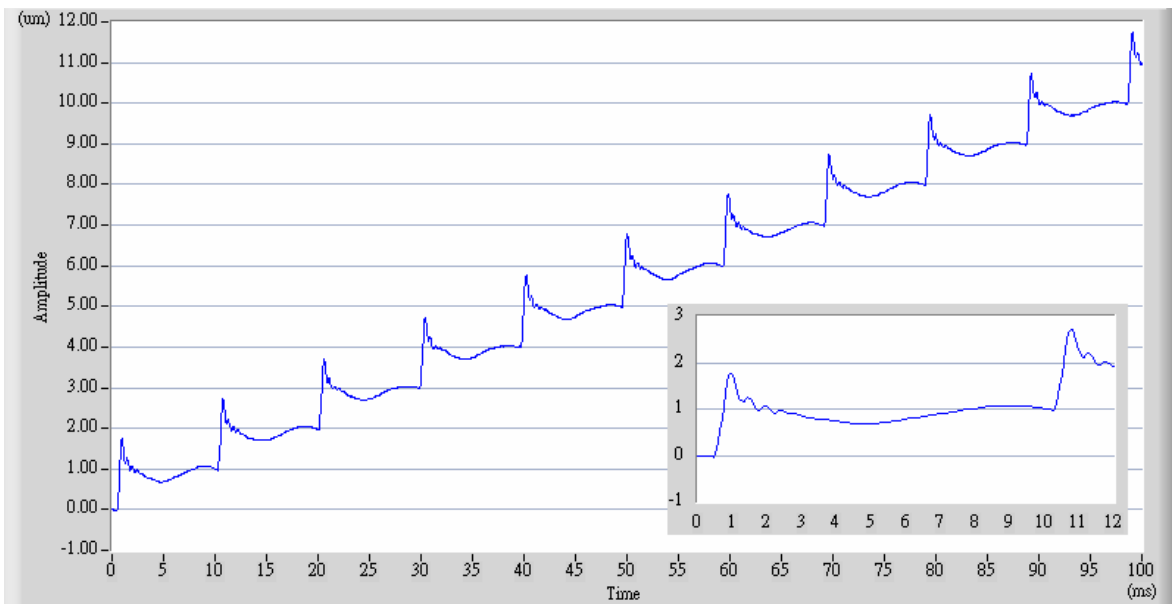


Figure 3.16 100V, 100Hz, 95% duty input, displacement of the slider

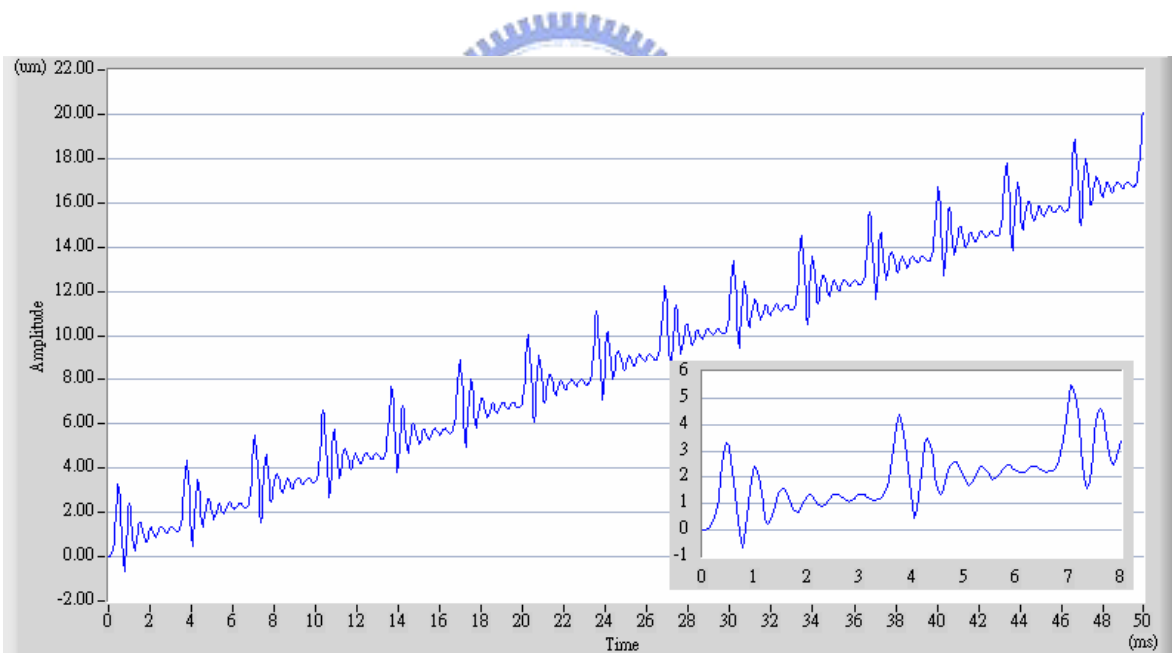


Figure 3.17 100V, 300Hz, 95% duty input, displacement of the slider

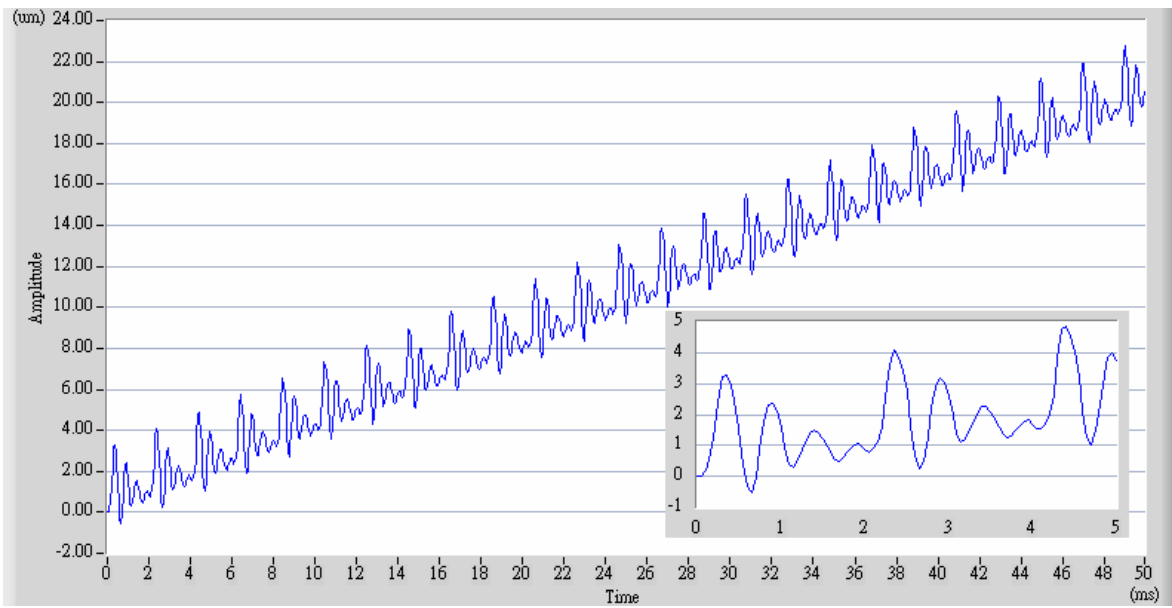


Figure 3.18 100V, 500Hz, 95% duty input, displacement of the slider

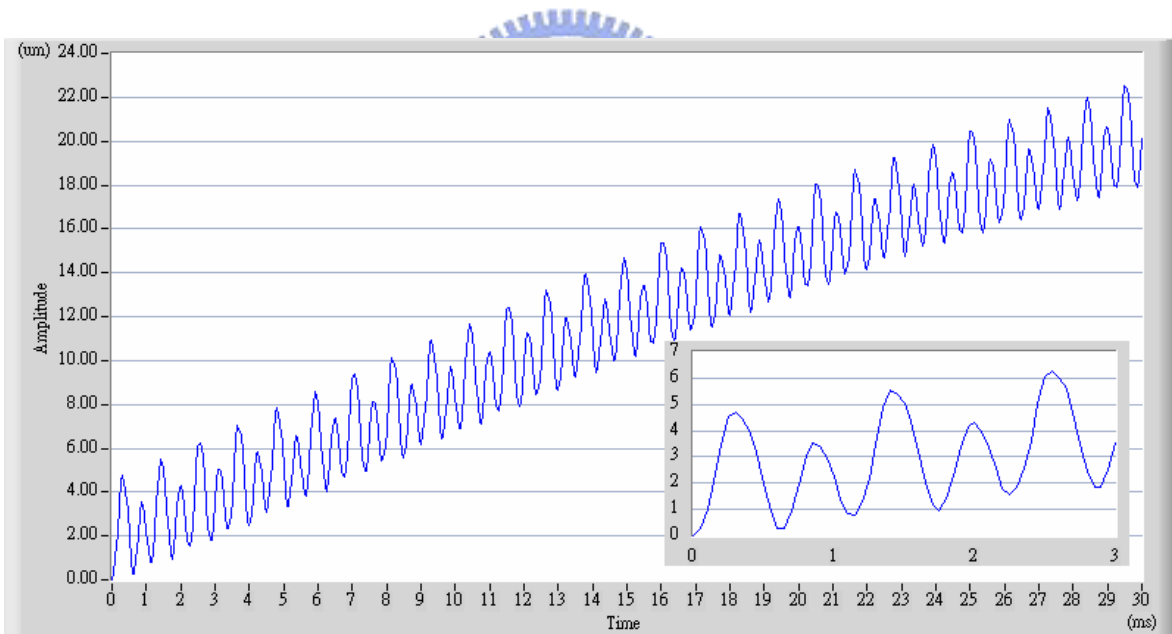


Figure 3.19 100V, 900Hz, 95% duty input, displacement of the slider

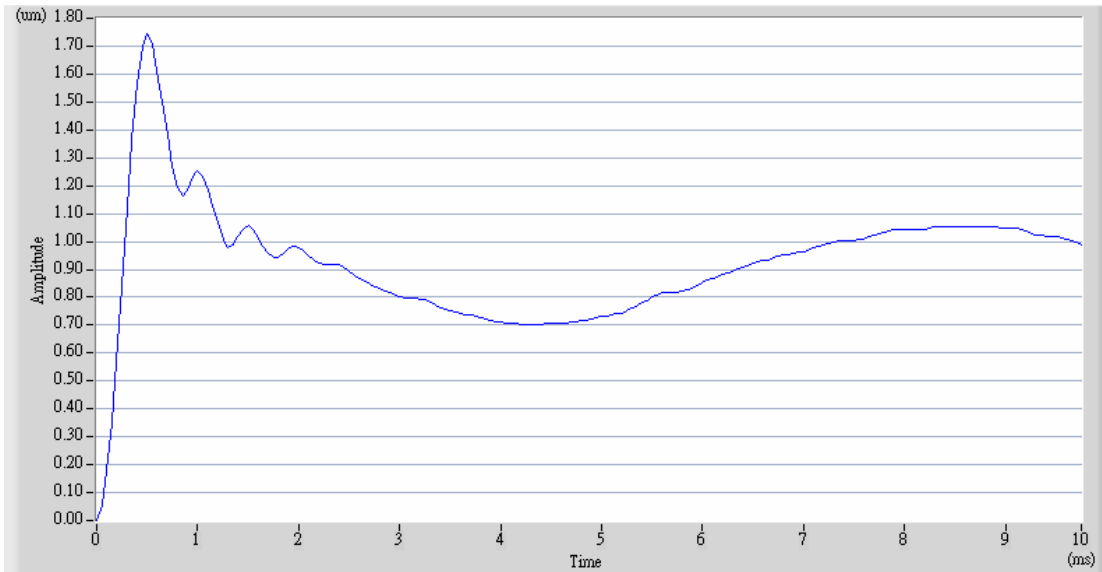


Figure 3.20 100V, 100Hz, 95% duty input, standard step of the slider

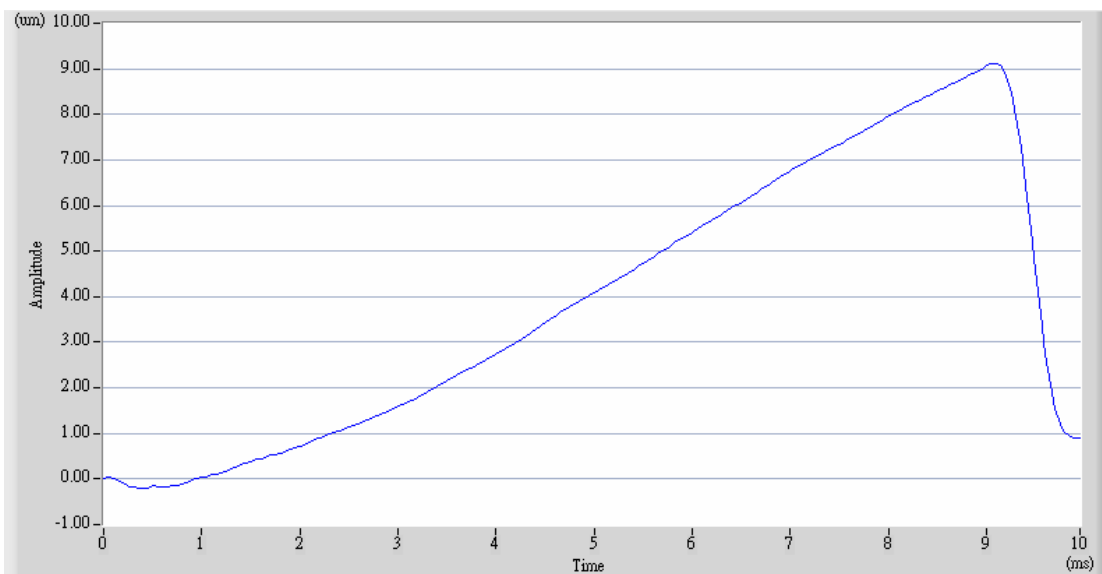


Figure 3.21 100V, 100Hz, 95% duty input, standard step of the counter-mass

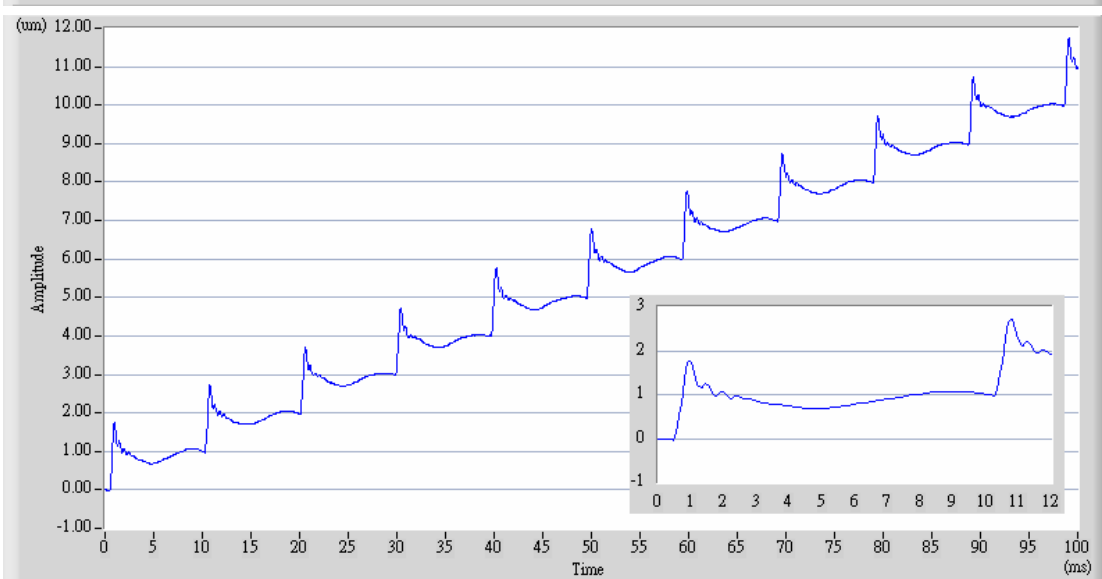
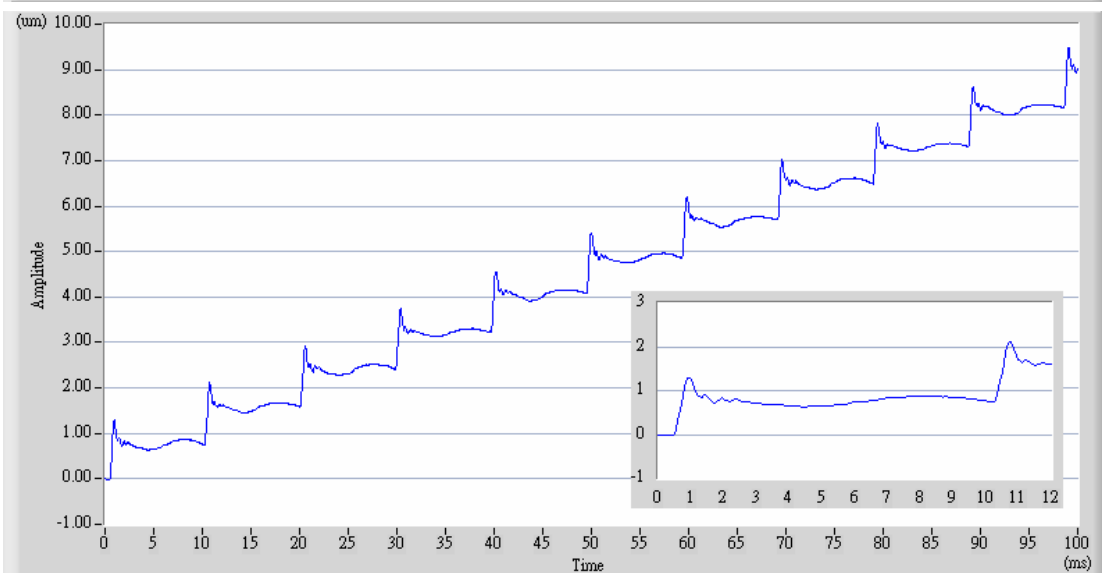
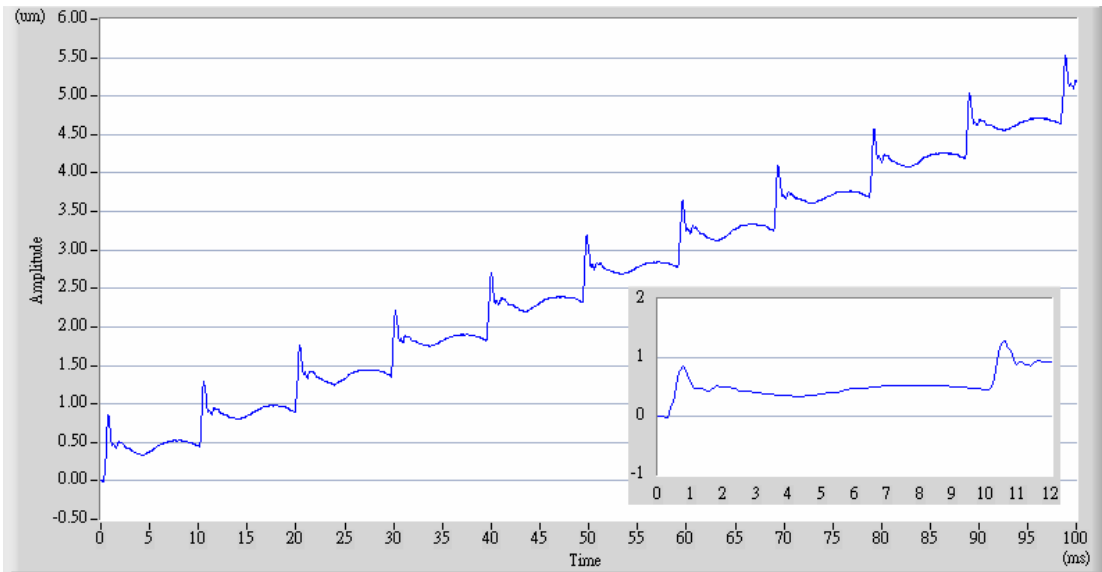


Figure 3.22 (a) 60V; (b) 80V; (c) 100V, 100Hz, 95% duty input, displacement of the slider

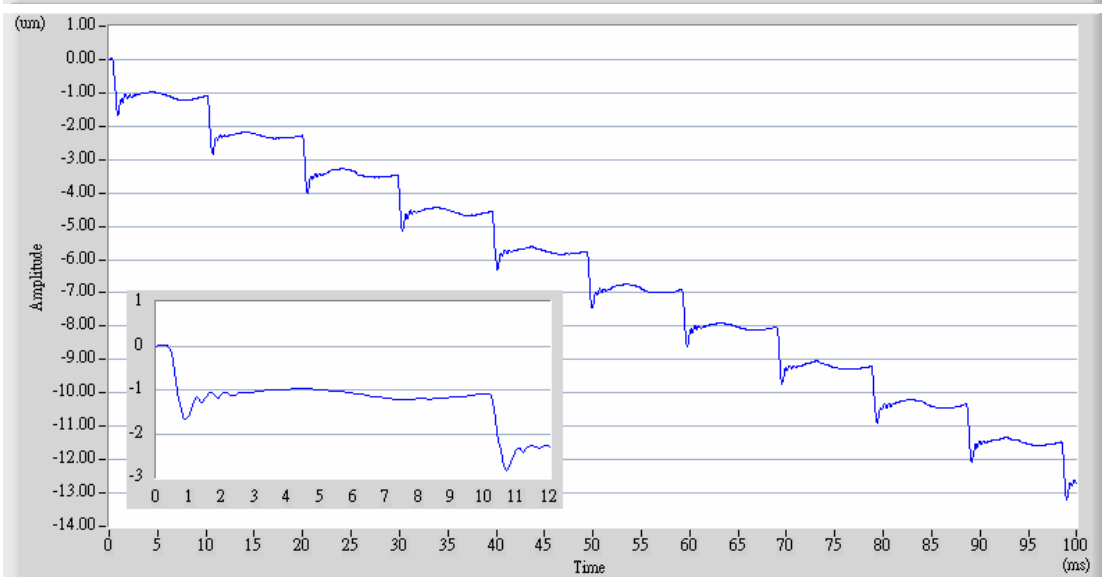
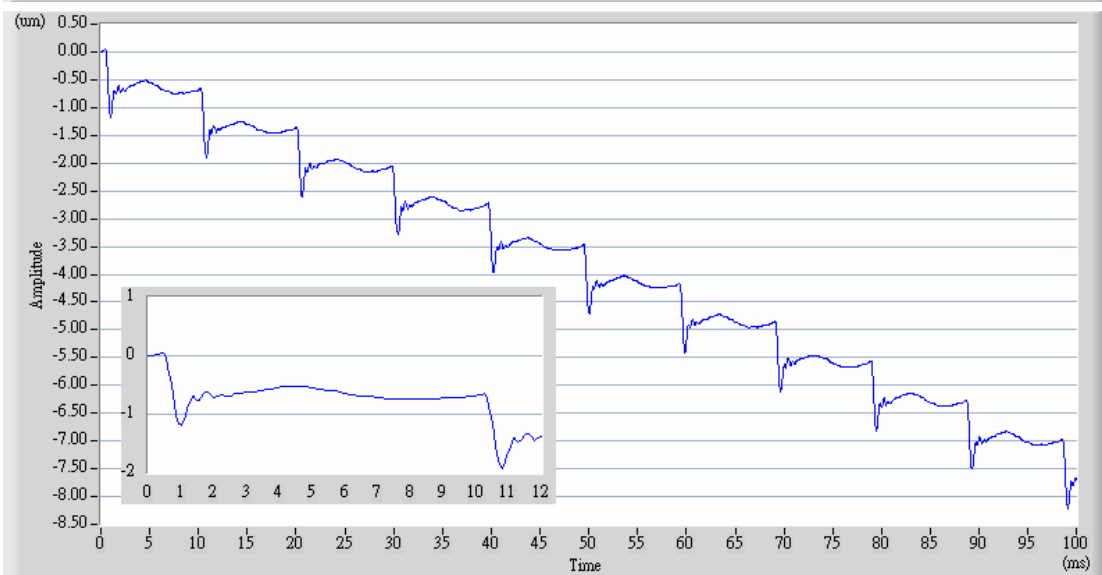
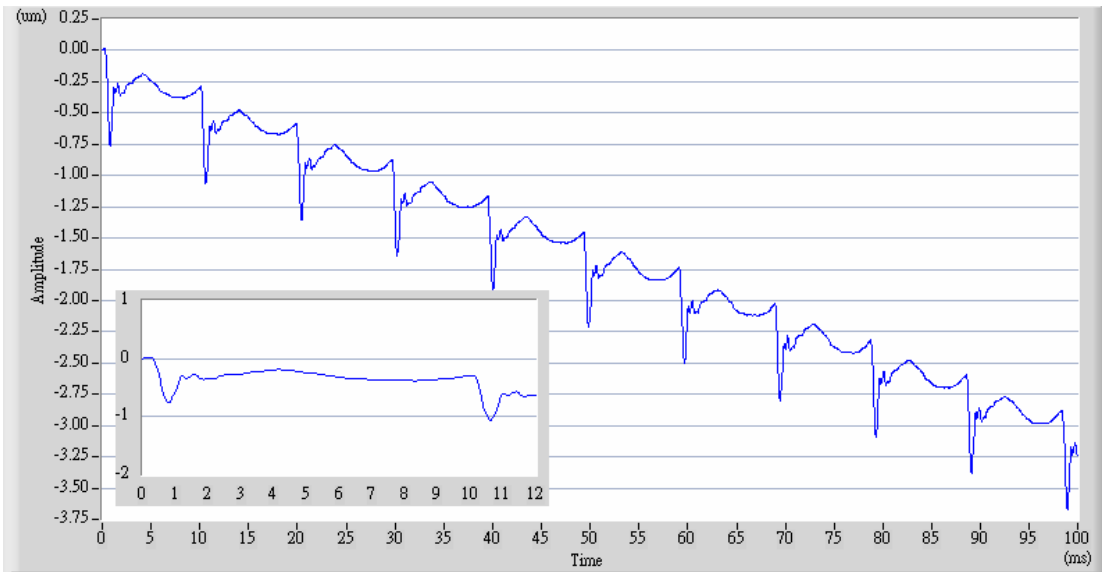


Figure 3.23 (a) 60V; (b) 80V; (c) 100V, 100Hz, 5% duty input, displacement of the slider

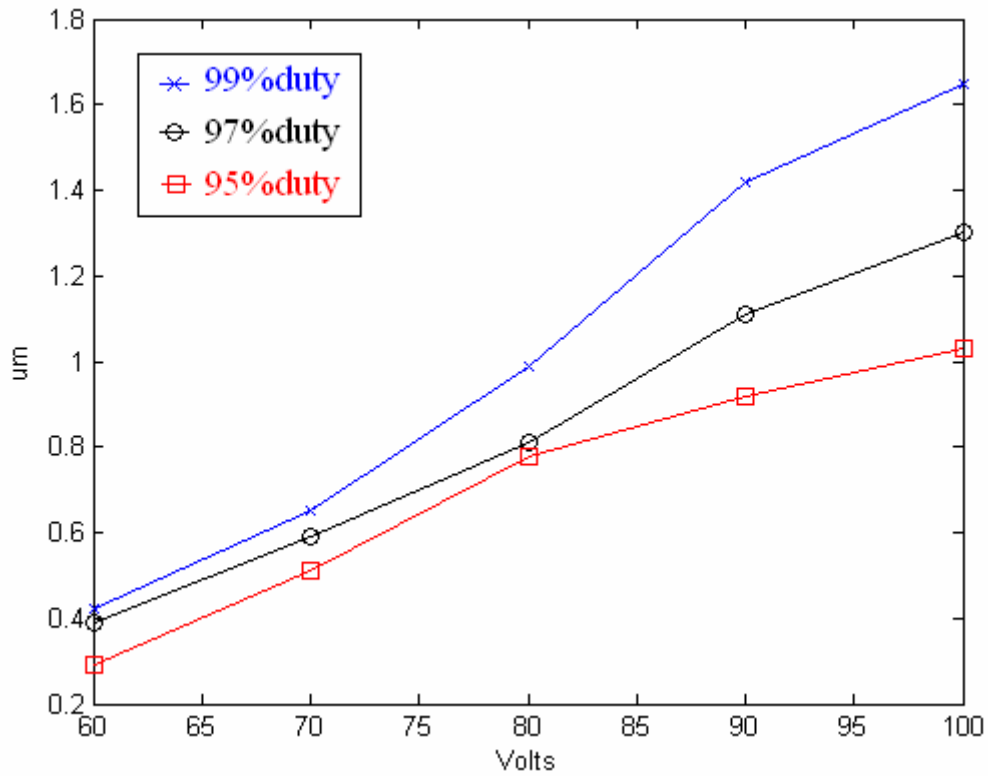


Figure 3.24 Forward displacement of the slider, 100Hz

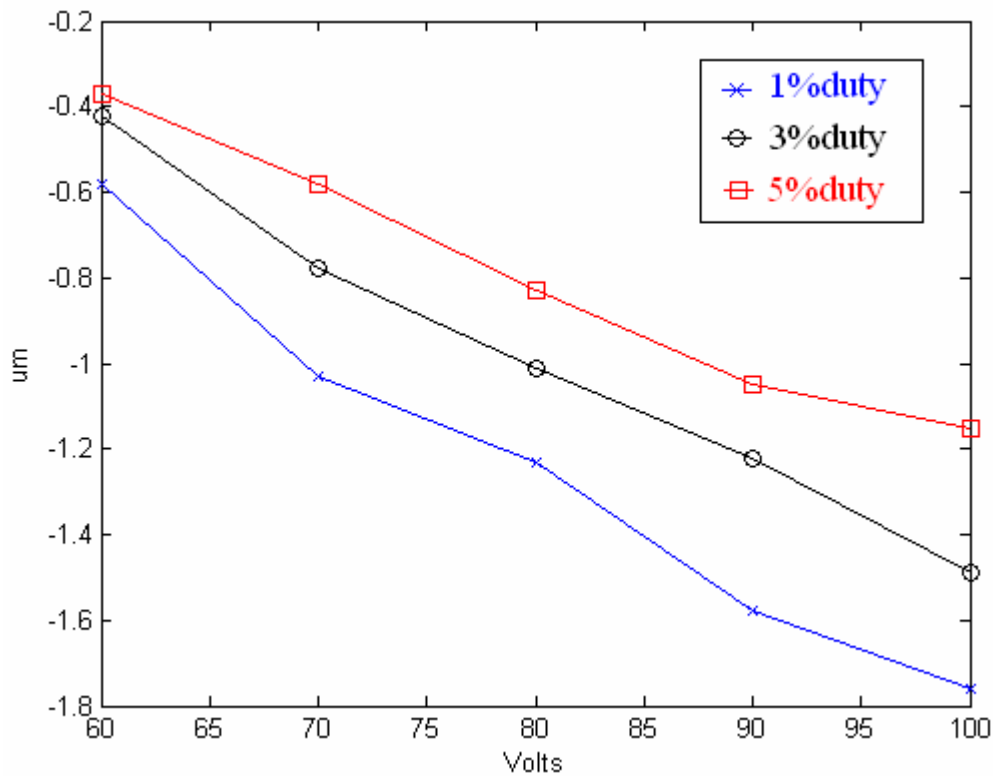


Figure 3.25 Backward displacement of the slider, 100Hz

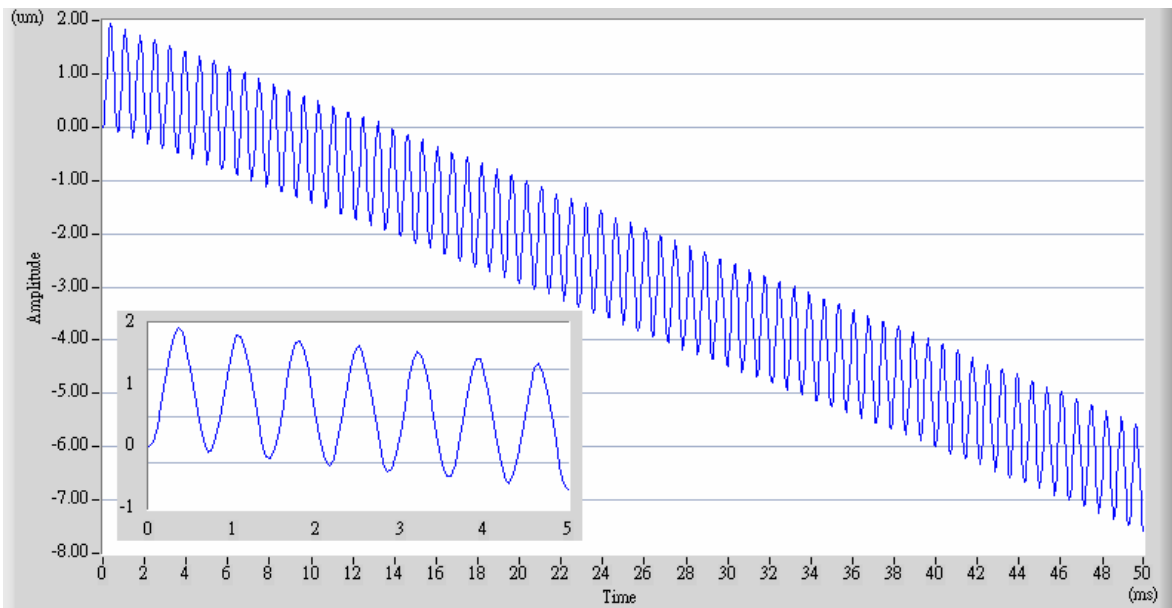


Figure 3.26 50V, 1400Hz, sine waveform input, displacement of the slider

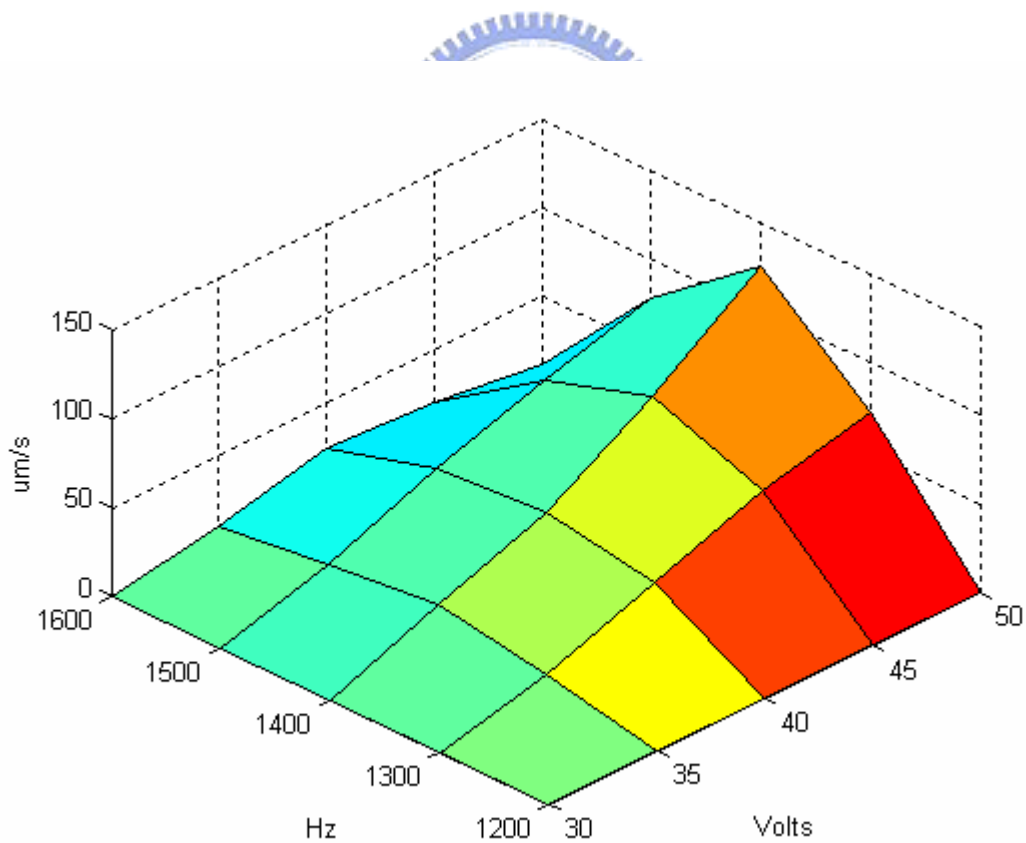


Figure 3.27 Velocity of the slider with various sine waveforms

Open-loop travel @ 0 to 100 V	15 μ m \pm 20%
Closed-loop / open-loop resolution	-/0.15nm
Static large-signal stiffness	57N/ μ m \pm 20%
Push/pull force capacity	1000/50N
Torque limit (at tip)	0.35Nm
Electrical capacitance	1.8 μ F \pm 20%
Dynamic operating current coefficient (DOCC)	15 μ A/ (Hz x μ m)
Unloaded resonant frequency (f ₀)	18kHz \pm 20%
Standard operating temperature range	-20 to +80°C
Voltage connection	VL
Weight without cables	20g \pm 5%
Material case / end pieces	N-S
Length L	32mm \pm 0.3

Table 3.1 Technical data of P-840.10 preloaded LVPZT translator

